



NAVAL POSTGRADUATE SCHOOL

MONTEREY, CALIFORNIA

THESIS

**AIR MOTOR INTEGRATION FOR A SMALL-SCALE
COMPRESSED AIR ENERGY STORAGE SYSTEM**

by

John D. McMahan

June 2021

Thesis Advisor:

Anthony J. Gannon

Co-Advisor:

Walter Smith

Approved for public release. Distribution is unlimited.

THIS PAGE INTENTIONALLY LEFT BLANK

REPORT DOCUMENTATION PAGE			<i>Form Approved OMB No. 0704-0188</i>	
Public reporting burden for this collection of information is estimated to average 1 hour per response, including the time for reviewing instruction, searching existing data sources, gathering and maintaining the data needed, and completing and reviewing the collection of information. Send comments regarding this burden estimate or any other aspect of this collection of information, including suggestions for reducing this burden, to Washington headquarters Services, Directorate for Information Operations and Reports, 1215 Jefferson Davis Highway, Suite 1204, Arlington, VA 22202-4302, and to the Office of Management and Budget, Paperwork Reduction Project (0704-0188) Washington, DC 20503.				
1. AGENCY USE ONLY (Leave blank)		2. REPORT DATE June 2021		3. REPORT TYPE AND DATES COVERED Master's thesis
4. TITLE AND SUBTITLE AIR MOTOR INTEGRATION FOR A SMALL-SCALE COMPRESSED AIR ENERGY STORAGE SYSTEM			5. FUNDING NUMBERS RMNPB	
6. AUTHOR(S) John D. McMahan				
7. PERFORMING ORGANIZATION NAME(S) AND ADDRESS(ES) Naval Postgraduate School Monterey, CA 93943-5000			8. PERFORMING ORGANIZATION REPORT NUMBER	
9. SPONSORING / MONITORING AGENCY NAME(S) AND ADDRESS(ES) Office of Naval Research, Arlington, VA, 22203			10. SPONSORING / MONITORING AGENCY REPORT NUMBER	
11. SUPPLEMENTARY NOTES The views expressed in this thesis are those of the author and do not reflect the official policy or position of the Department of Defense or the U.S. Government.				
12a. DISTRIBUTION / AVAILABILITY STATEMENT Approved for public release. Distribution is unlimited.			12b. DISTRIBUTION CODE A	
13. ABSTRACT (maximum 200 words) <p>The lack of on-demand energy production capabilities, paired with the lack of sufficient battery technology, has been a major issue for renewable energy source viability. Compressed Air Energy Storage (CAES) offers the potential to mitigate the latter challenge with a safe, robust, and cost-effective method of storing excess renewable energy at the microgrid level. Positive displacement radial air motors serve as one potential method of extracting the energy back from the compressed air. This thesis aims to integrate such a motor with a corresponding control scheme into a small-scale CAES system to allow autonomous operation of the microgrid during times of little to no solar power availability. The motor would utilize the compressed air to maintain sufficient charge across the bank of a capacitor-based microgrid. Successful integration would help verify the capability of a small-scale CAES system in providing a resilient and environmentally friendly microgrid.</p>				
14. SUBJECT TERMS Compressed Air Energy Storage, CAES, air motor, super-capacitor, energy extraction, energy storage			15. NUMBER OF PAGES 73	
			16. PRICE CODE	
17. SECURITY CLASSIFICATION OF REPORT Unclassified	18. SECURITY CLASSIFICATION OF THIS PAGE Unclassified	19. SECURITY CLASSIFICATION OF ABSTRACT Unclassified	20. LIMITATION OF ABSTRACT UU	

THIS PAGE INTENTIONALLY LEFT BLANK

Approved for public release. Distribution is unlimited.

**AIR MOTOR INTEGRATION FOR A SMALL-SCALE COMPRESSED AIR
ENERGY STORAGE SYSTEM**

John D. McMahan
Ensign, United States Navy
BS, United States Naval Academy, 2020

Submitted in partial fulfillment of the
requirements for the degree of

MASTER OF SCIENCE IN MECHANICAL ENGINEERING

from the

**NAVAL POSTGRADUATE SCHOOL
June 2021**

Approved by: Anthony J. Gannon
Advisor

Walter Smith
Co-Advisor

Garth V. Hobson
Chair, Department of Mechanical and Aerospace Engineering

THIS PAGE INTENTIONALLY LEFT BLANK

ABSTRACT

The lack of on-demand energy production capabilities, paired with the lack of sufficient battery technology, has been a major issue for renewable energy source viability. Compressed Air Energy Storage (CAES) offers the potential to mitigate the latter challenge with a safe, robust, and cost-effective method of storing excess renewable energy at the microgrid level. Positive displacement radial air motors serve as one potential method of extracting the energy back from the compressed air. This thesis aims to integrate such a motor with a corresponding control scheme into a small-scale CAES system to allow autonomous operation of the microgrid during times of little to no solar power availability. The motor would utilize the compressed air to maintain sufficient charge across the bank of a capacitor-based microgrid. Successful integration would help verify the capability of a small-scale CAES system in providing a resilient and environmentally friendly microgrid.

THIS PAGE INTENTIONALLY LEFT BLANK

TABLE OF CONTENTS

I.	INTRODUCTION.....	1
A.	DON ENERGY STRATEGY.....	1
B.	FUTURE OF RENEWABLES	1
C.	RENEWABLE LIMITATIONS	2
D.	CAES SYSTEMS	3
1.	Utility–Scale.....	3
2.	Small-Scale Systems.....	5
E.	SOLAR-CAES MICROGRID	6
F.	EXPANSION SYSTEM	6
G.	MOTIVATION AND APPROACH	7
II.	MICROGRID COMPONENTS	9
A.	SOLAR PANELS AND CONTROLLER.....	10
B.	INVERTER AND TRANSFORMER	12
C.	CAPACITOR BANK AND POWER SUPPLY	13
D.	CAPACITOR UPGRADE.....	14
1.	Capacitor Comparison	14
2.	Capacitor Bank Reconfiguration.....	16
III.	AIR MOTOR CONFIGURATION.....	19
A.	MOTOR GENERATION MODULE.....	19
B.	CONTROL MANIFOLD	20
IV.	MOTOR CHARGE CHARACTERISTICS AND CONTROL.....	23
A.	MOTOR INSTRUMENTATION.....	23
B.	TESTING.....	24
C.	SYSTEM CONTROLLER.....	25
D.	INITIAL EXPANSION CODE.....	26
V.	MOTOR INTEGRATION AND MICROGRID CONTROL.....	29
A.	AIR MOTOR CONNECTION	29
B.	CONTROL MODIFICATIONS.....	31
C.	EXPERIMENTAL TESTING	34
VI.	RESULTS AND DISCUSSION	35
A.	MOTOR CHARGE RESULTS	35
B.	DISCUSSION	39

C.	MICROGRID RESULTS AND DISCUSSION.....	39
D.	DISCUSSION	40
VII.	CONCLUSION	41
APPENDIX A. MATLAB CODES.....		43
A.	DATA ACQUISITION.....	43
B.	DATA FILTER	45
APPENDIX B. CCW CONTROL CODE.....		47
A.	VOLTAGE CONTROL	47
B.	VOLTAGE SCALE	48
C.	GLOBAL VARIABLES	48
APPENDIX C. LOCAL STATUS PANEL APP.....		49
A.	ACQUISITION	49
B.	PLOTTING	50
LIST OF REFERENCES		51
INITIAL DISTRIBUTION LIST		53

LIST OF FIGURES

Figure 1.	Average Construction Costs for Electricity Generators. Source: [3].	2
Figure 2.	Planned Electrical Generating Capacity. Source: [4].	2
Figure 3.	CAES Plant Schematic. Source: [5].	3
Figure 4.	System Power Rating and Discharge of Storage Technologies. Source: [5].	4
Figure 5.	Small Scale CAES System. Source: [5].	5
Figure 6.	Simplified Microgrid Schematic.	9
Figure 7.	SS-CAES Electrical System Architecture. Source: [8].	10
Figure 8.	SS-CAES Solar Panel Array. Source [8].	11
Figure 9.	Midnite Classic 150 Charge Controller.	11
Figure 10.	SMA Sunny Island Inverter.	12
Figure 11.	SMA Sunny Island Smartformer.	13
Figure 12.	BK Precision 1550 Power Supply Module.	14
Figure 13.	SkelMod 51V 177F Ultracapacitor Module. Source: [11].	14
Figure 14.	Capacitor Size Comparison.	16
Figure 15.	Updated Capacitor Configuration (side view).	17
Figure 16.	Updated Capacitor Configuration (front view).	18
Figure 17.	UTAM4-030S Cutaway Schematic. Adapted from [13].	19
Figure 18.	UTAM4-030S Operating Curves. Adapted from [13].	19
Figure 19.	Air Motor Assembly.	20
Figure 20.	Expansion Control Manifold. Adapted from [10].	21
Figure 21.	Motor Side Data Acquisition.	23
Figure 22.	Computer Side Data Acquisition.	24

Figure 23.	Allen Bradley Micro 850 PLC.....	25
Figure 24.	Micro 850 Wired Connections.....	26
Figure 25.	Block Form SCALER Function. Source: [10]......	27
Figure 26.	Structured Test SCALER Function.	27
Figure 27.	Previous Power Supply Connection.....	29
Figure 28.	Motor-Grid Connection.	30
Figure 29.	Controller, Manifold, and Motor Setup.	31
Figure 30.	Activate_PowerSupply Sub-Program. Source: [8].	32
Figure 31.	Activate_PowerSupply Sub-Program Modifications.....	33
Figure 32.	Plot of Voltage vs. Time.	35
Figure 33.	Plot of Current vs. Time.....	36
Figure 34.	Plot of Power vs. Time.....	36
Figure 35.	Plot of Air Pressure vs. Time.....	37
Figure 36.	Plot of Motor Speed vs. Time.	38
Figure 37.	Microgrid Integration Verification.	40

LIST OF TABLES

Table 1.	Capacitor Characteristics of Maxwell and SkelMod Variants. Adapted from [11], [12].	15
----------	--	----

THIS PAGE INTENTIONALLY LEFT BLANK

LIST OF ACRONYMS AND ABBREVIATIONS

CAES	compressed air energy storage
MPPT	maximum power point tracking
MWe	megawatts electric
NI DAQ	National Instrumentation data acquisition
PLC	programmable logic controller
RPM	revolutions per minute
SSR	solid-state relay
SS-CAES	small-scale compressed air energy storage
VDC	voltage direct current
VAC	voltage alternating current

THIS PAGE INTENTIONALLY LEFT BLANK

NOMENCLATURE

C	Capacitance	F
C_p	specific heat	$J/kg\cdot K$
E_{in}	energy entering the air motor	J
E_{stored}	maxed stored energy	J
V	voltage	V
ρ	density	kg/m^3
γ	specific heat ratio	-

THIS PAGE INTENTIONALLY LEFT BLANK

ACKNOWLEDGMENTS

I would like to acknowledge my family for their unwavering support as I have pursued my academic interests.

THIS PAGE INTENTIONALLY LEFT BLANK

I. INTRODUCTION

A. DON ENERGY STRATEGY

The Department of the Navy released their Installation Energy Resilience Strategy in February of 2020 with the intent to continually improve its energy security and capability at all times. Its formulation draws from two specific issues detailed in the February 2018 National Defense Strategy. Namely, it acknowledges that America is no longer immune to the various attacks and interference from those who wish it harm and that every domain, to include cyberspace, is heavily contested by near peer adversaries. This poses a direct risk to America's energy security and contributes to the Navy's previous Energy Security Framework's goal of improving the resilience, reliability, and efficiency of its aging energy infrastructure [1].

B. FUTURE OF RENEWABLES

Much of the needed infrastructure improvement and creation revolves around renewable energy. The past decade saw a large increase in renewable technology implementation in Naval installations due to the energy goals put forward by Secretary Mabus in 2009. One goal in particular aimed at producing 50% of shore-based installation energy requirements through renewable means by 2020 [2]. This clean energy initiative has been aided by the continual scientific and economic development of well-established renewable technology. Average construction costs for solar photovoltaic generators alone dropped 50% between 2013 and 2018, as seen in Figure 1 [3]. Renewables even account for most of the new U.S. electricity generating capacity in 2021, with 39.7 gigawatts becoming operational. Of that, solar comprises 39% with a planned 15.4-gigawatt addition to the grid. Figure 2 shows a complete breakdown of the various generators coming online [4].

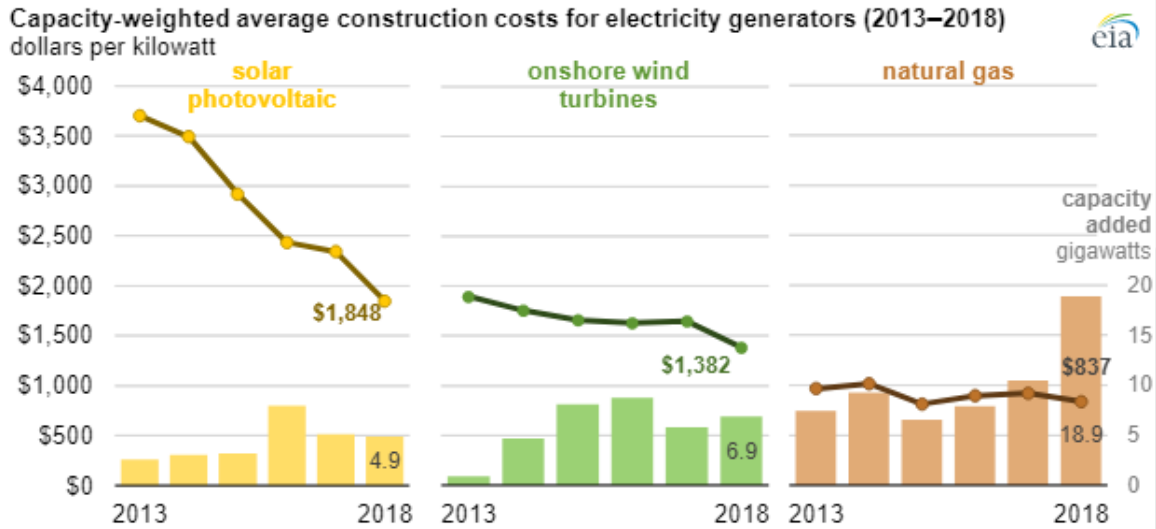


Figure 1. Average Construction Costs for Electricity Generators. Source: [3].

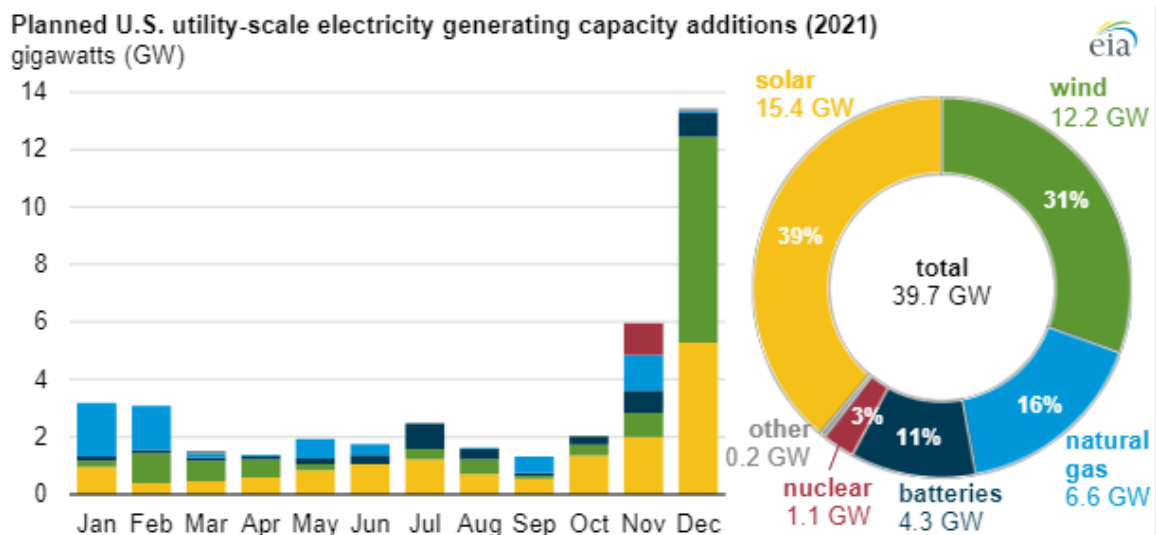


Figure 2. Planned Electrical Generating Capacity. Source: [4].

C. RENEWABLE LIMITATIONS

However, fluctuating environmental conditions create a substantial obstacle for certain renewable technologies. The energy production from solar panels and wind turbines is at the mercy of the weather. Long-term seasonal trends can be predicted for given geographical locations, but the day-to-day operation is subject to much uncertainty. A lack of wind or sunshine can effectively shut down a grid reliant on these systems. Even in ideal

conditions, the technology is still limited as these renewables are incapable of load following. During peak energy consumption times, consumer demand could surpass production with no means of closing the gap. Likewise, at times of low demand, any excess energy produced is wasted. Thus, development of storage methods is essential in mitigating these issues and making renewable energy a viable option.

D. CAES SYSTEMS

1. Utility-Scale

CAES has been around for the better part of 50 years gaining significant traction in the 1970s for its use in the nuclear power industry. Excess electricity produced during times of low demand would be used to compress air into large underground caverns. When demand increased, the air would be released and sent through turbine machinery to recover the stored electricity. A general schematic of the CAES process is shown in Figure 3.

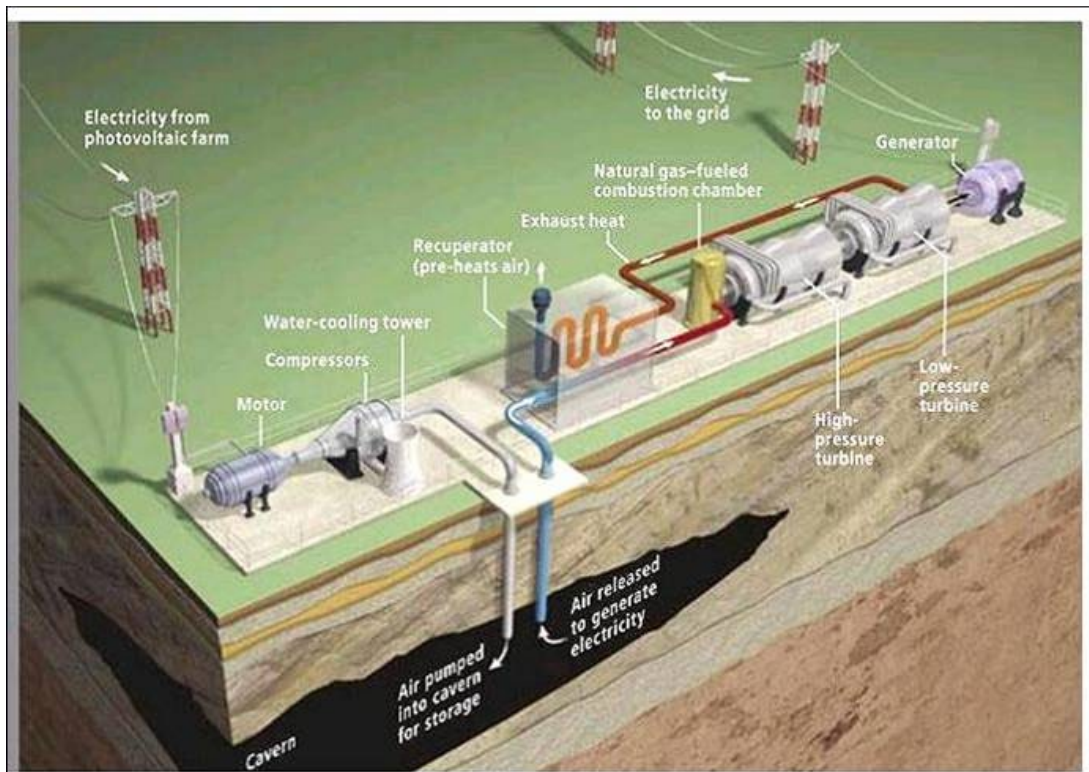


Figure 3. CAES Plant Schematic. Source: [5].

Currently, large-scale (~100-300 MWe) CAES plants exist in Huntorf, Germany, and McIntosh, Alabama, providing decades of operational experience and technological viability. CAES systems even offer one of the highest system power ratings of any current storage medium, rivaling that of batteries and hydroelectricity. While slower in its overall discharge rate compared to its competitors, CAES's ability to produce consistent energy support for several hours if needed (Figure 4).

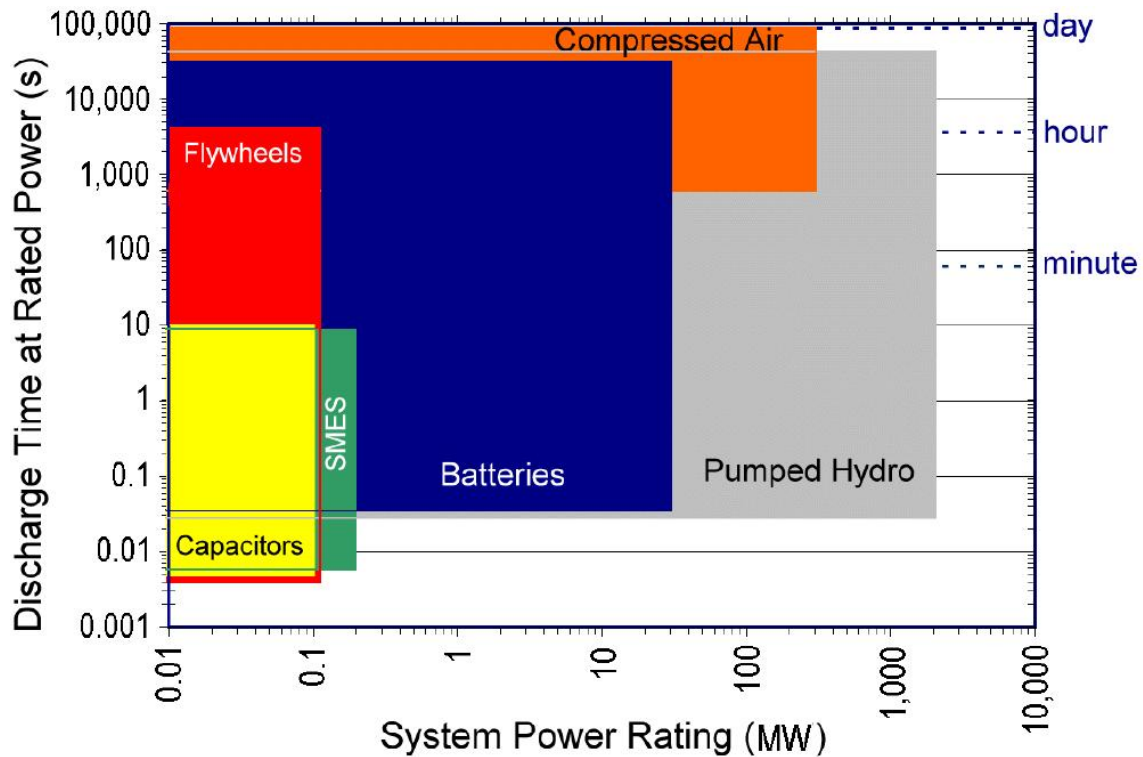


Figure 4. System Power Rating and Discharge of Storage Technologies.
Source: [5].

One perceived drawback of this method of storage is the lack of underground geology requirements for suitable CAES sites. But, according to a study performed by the Electric Power Research Institute in 2002, approximately 80% of U.S. states contain adequate conditions for development [5].

2. Small-Scale Systems

Despite contentions regarding large-scale CAES feasibility, the technology has been readily adapted to meet small-scale operations through the use of high-pressure storage tanks above ground. The expansion side shown in Figure 5 adheres to the same principles of its larger counterparts. Compressed air, assisted by natural gas, is sent through a combustion turbine to create electricity [5].



Figure 5. Small Scale CAES System. Source: [5].

This method could be readily integrated into the Navy's existing pneumatic infrastructure on both ships and shore installations. Although, the need of natural gas still proves problematic to the reliability, resilience, and efficiency of these systems as supply chains can be disrupted. A lack of fuel would severely reduce or even prevent electrical generation from the turbines. Removing combustion from the process by replacing the

turbines with positive displacement expanders was explored by He and Wang. Their work focused on the optimal selection of air expansion technology for CAES. In it they noted the increased efficiency, smaller size, and lower rotational speeds rotary expanders produced for small scale operations compared to traditional turbines [6].

E. SOLAR-CAES MICROGRID

The implementation and control of a renewable small scale compressed air energy storage (SS-CAES) microgrid at the Naval Postgraduate School Turbo Lab is laid out in work done most recently by Tan and Williams. Williams designed much of the compression control system that relied on an array of solar panels to power the microgrid. The first strand of parallel panels was designed to charge and maintain the voltage level on a bank of ultracapacitors as a form of temporary energy storage. Doing this allowed the compression system to run when solar conditions proved sub-optimal [7].

Tan took the automation of the compression system a step further with the addition of an alternate power supply. During the night, the capacitor bank that provided energy for the microgrid components would slowly discharge. If the voltage level dropped below 30 V, the inverter would enter a self-protection mode and would require a manual reset the next day. Tan integrated a power supply module that would maintain sufficient voltage levels across the capacitors to prevent shutdown. The accompanying code that controlled its connection to the microgrid served as a steppingstone for full expansion system integration [8].

F. EXPANSION SYSTEM

Radial air piston motors were proposed by Johnson and his predecessors as a means of generating electricity from compressed air. The motors used for analysis were acquired from AirOil Systems and outfitted with two different electric generators. Johnson tested the performance of the motor with an 80 kV and 150 kV generator and compared their efficiencies to past expansion modules. A major factor Johnson explored was the effect of pressure and air consumption on motor efficiency. Johnson analysis confirmed the 80 kV generator to be the most suitable choice for the motor application [9].

While Johnson refined the means of generating electricity from compressed air, Vranas designed a control code and manifold for regulating the motor's output. Two separate channels within the piping were created and regulated through solenoid valves and a manual lever. The solenoid valves could be opened or closed through the use of electric signals sent from a controller. Thus, the code could start and stop the motor's charging ability based on an input reading of the capacitor's voltage level [10].

G. MOTIVATION AND APPROACH

The significant development in design and control of both the expansion and compressions systems at NPS over the past years has reached a culmination. The microgrid's automated control paired with its alternate power source capability provides optimal conditions for the integration of the radial air motor and control manifold. The compressed air architecture and use of capacitors as short-term storage finally allows for a "Dark-start" capability, as capacitors can continuously be recharged from zero volts unlike traditional batteries.

Before successful integration could take place, the microgrid had to be updated in several ways to support better temporary storage capabilities and control of the new expansions system. The motor's charging characteristics had to be explored as well due to a change in capacitor technology and air supply pressure drops.

THIS PAGE INTENTIONALLY LEFT BLANK

II. MICROGRID COMPONENTS

The microgrid's main purpose is to provide a source of renewable energy that can be efficiently stored and rapidly released upon demand. As previously mentioned, a collection of 12 solar panels serves as the primary means of energy production, while storage tanks hold the excess energy in the form of compressed air.

A simplified schematic of the major microgrid components necessary in accomplishing the task are depicted in Figure 6. The dotted red lines represent upgrades and modifications to the microgrid discussed in later sections. An actual image of the microgrid with the additional safety and control components is included in Figure 7.

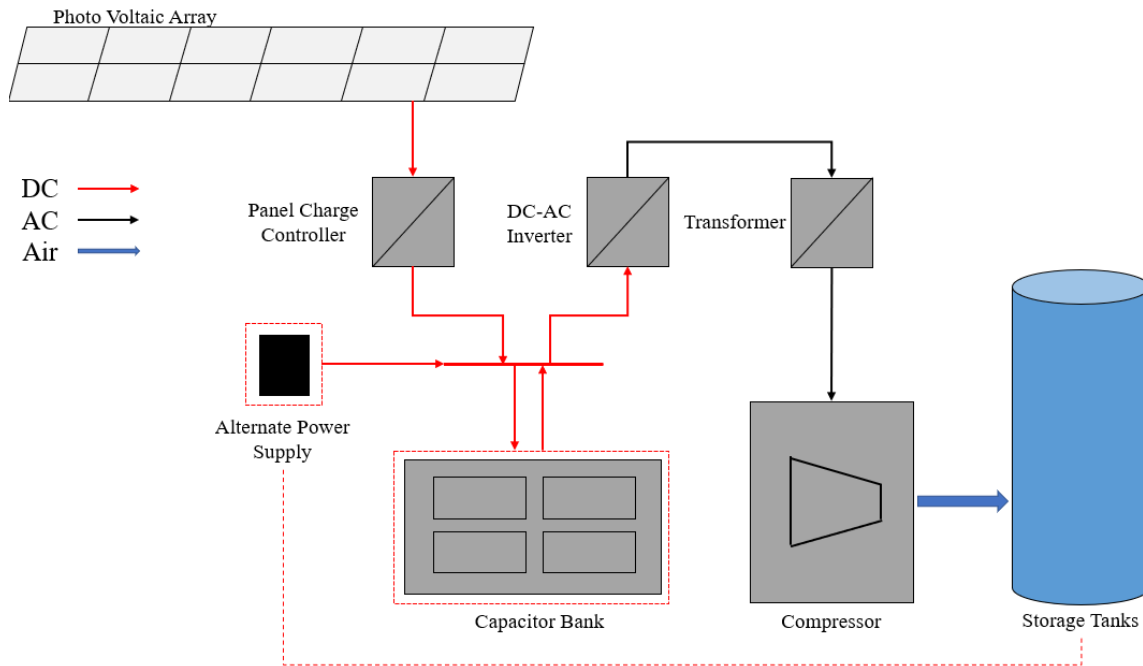


Figure 6. Simplified Microgrid Schematic.

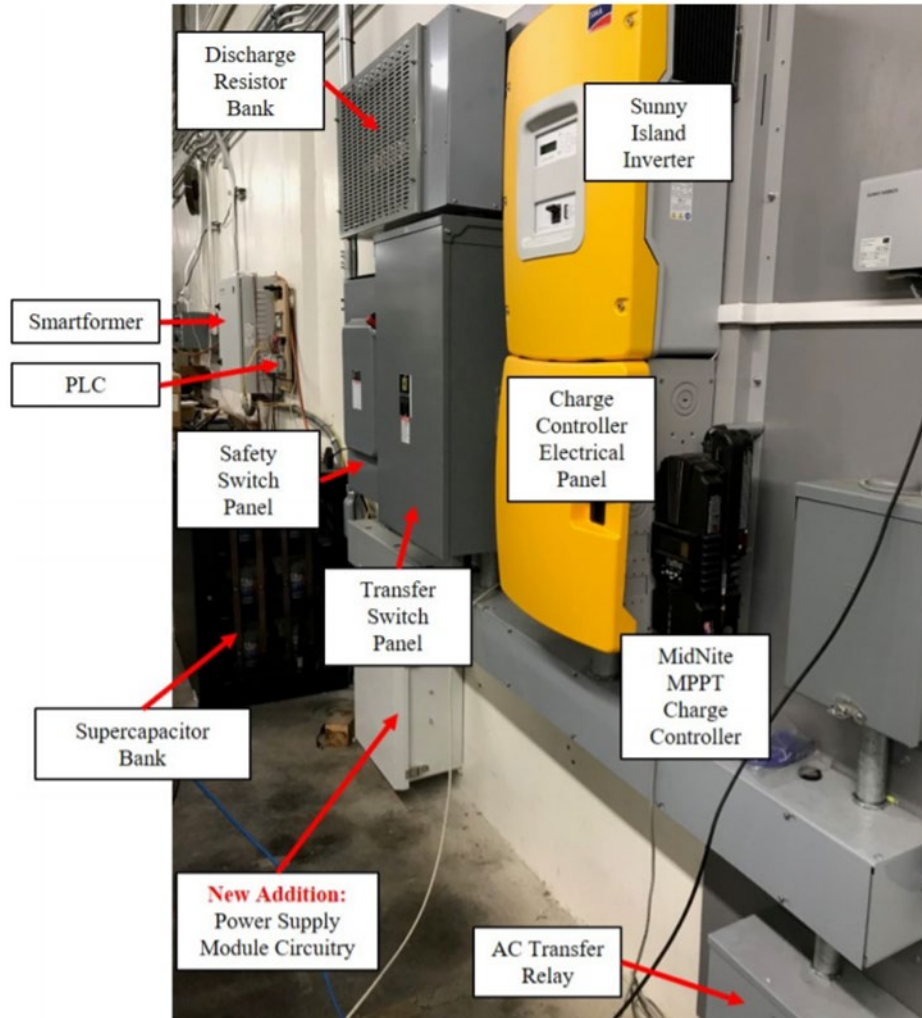


Figure 7. SS-CAES Electrical System Architecture. Source: [8]

A. SOLAR PANELS AND CONTROLLER

The microgrid draws its power from a 12-panel photovoltaic array mounted directly on the building in which the grid is housed. The first strand is comprised of two panels in parallel that directly charge the capacitor bank to bring the microgrid's electronics online thus enabling a "Dark-start" capability. The remaining five strands of two panels in series are dedicated to running the compressor and filling the compressed air tanks.

The configuration of the solar array is broken down in Figure 8. Once the capacitor bank reaches sufficient charge, the Midnite Classic 150 charge controller comes online and begins regulating the panels' power output to the microgrid.

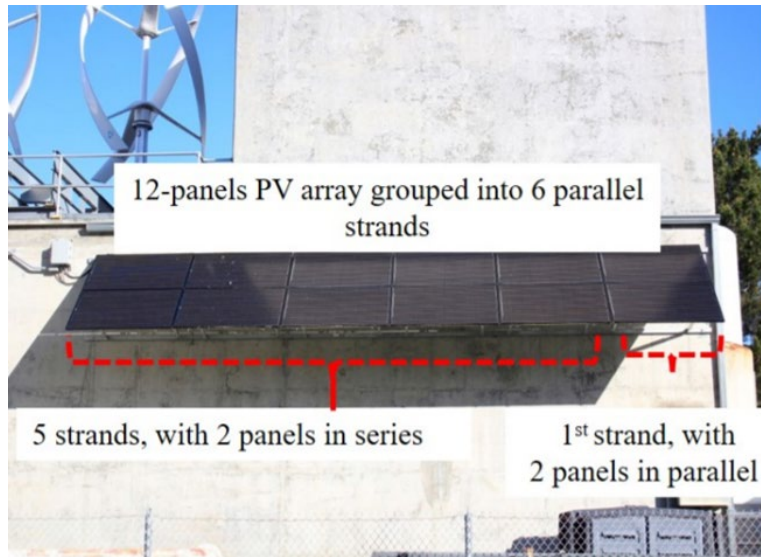


Figure 8. SS-CAES Solar Panel Array. Source [8].

The charge controller pictured in Figure 9 utilizes its Maximum Power Point Tracking (MPPT) algorithm to maximize voltage and current outputs to both the capacitor bank and inverter. Once fully charged, the controller maintains the voltage level of the capacitors through float charging.



Figure 9. Midnite Classic 150 Charge Controller.

B. INVERTER AND TRANSFORMER

The SMA Sunny Island Inverter serves as an essential component to the operation of the microgrid. Voltage directly from the solar panel array or capacitor bank must be converted from VDC to VAC for the compressor to function.

The 6 kW inverter shown in Figure 10 produces 120 VAC from the incoming supply before it passes through the SMA Sunny Island Smartformer. The step-up transformer in Figure 11 then converts the 120 VAC to 240 VAC to power the compressor.



Figure 10. SMA Sunny Island Inverter.



Figure 11. SMA Sunny Island Smartformer.

C. CAPACITOR BANK AND POWER SUPPLY

The capacitor bank serves two main purposes during microgrid operation. The first consists of providing power to all microgrid electronics. This alone is why there is a dedicated solar panel strand for charging the capacitors. Without sufficient charge many of the components, to include the Midnite Classic 150 and SMA Inverter, would shut down. The inverter would also need a fifteen-minute manual reset before operation could resume. The second purpose is to provide a readily available short term electrical storage medium for devices being powered from the microgrid.

Overnight the capacitors are drained by the microgrid components they power. Tan used the BK Precision 1550 Power Supply Module shown in Figure 12, which when activated, maintained a voltage of 36 V [8]. The power supply served only as a temporary place holder as a substitute for an air powered generation system as it relied on power from the main grid.



Figure 12. BK Precision 1550 Power Supply Module.

D. CAPACITOR UPGRADE

1. Capacitor Comparison

Issues with the previous capacitor configuration and subsequent malfunction of a few units led to the search for a more advanced variant. Skeleton Technologies' SkelMod 51 V 177 F Ultracapacitor Module, pictured in Figure 13, was chosen to replace the Maxwell capacitors previously in use.



Figure 13. SkelMod 51V 177F Ultracapacitor Module. Source: [11].

The slight reduction in maximum voltage level would normally reduce the total stored energy according to Equation 1; however, the much higher capacitance rating makes up for the slight voltage decrease. The total energy is a function of the capacitance, C , and the voltage, V .

$$E_{stored} = \frac{1}{2} CV^2 \quad (1)$$

A comparison of several key capacitor specifications between the previous and new capacitors is provided in Table 1.

Table 1. Capacitor Characteristics of Maxwell and SkelMod Variants.
Adapted from [11], [12].

	Maxwell	SkelMod
Voltage	56 V	51 V
Capacitance	130 F	177 F
Energy	56.6 Wh	63.9 Wh
Energy Density	2.7 Wh/L	4.7 Wh/L

The energy density alone makes the newer capacitors ideal for small-scale applications. Figure 14 highlights the overall smaller physical dimensions the new capacitors' offer.

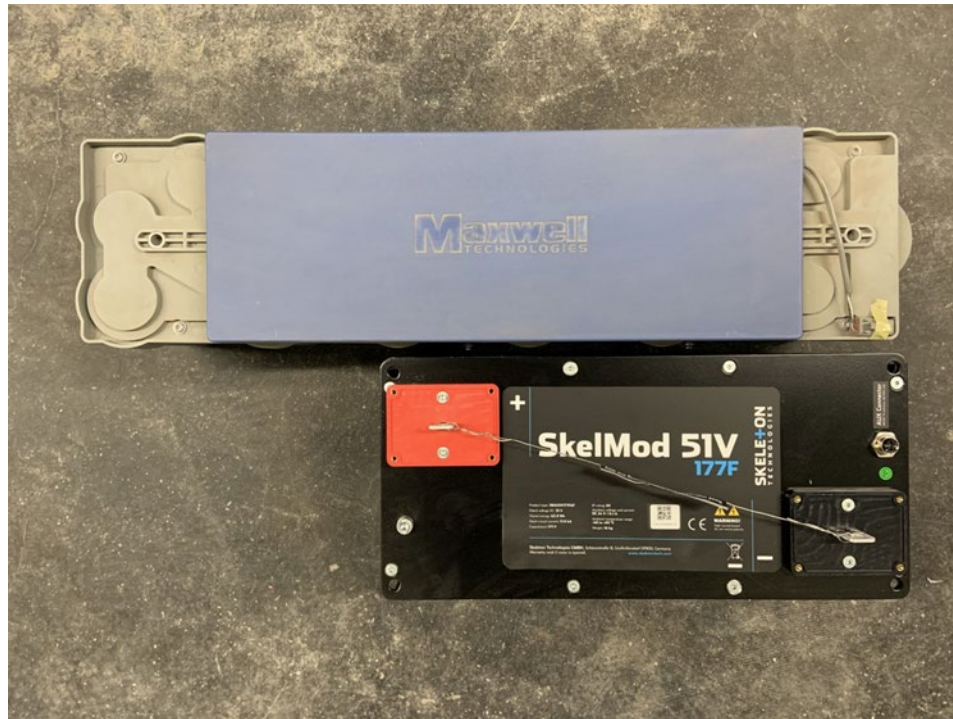


Figure 14. Capacitor Size Comparison.

2. Capacitor Bank Reconfiguration

The past configuration utilized the front oriented threaded terminals as the structural support for the copper bus bar. The setup provided direct and isolated charge connections for both the positive and negative terminals. Significant modification was required with the replacement due to the overall capacitor size and terminal configuration.

The smaller package made it more practical to rotate the capacitors 90 degrees so that each unit spanned the width of the housing structure as seen in Figure 15. Only four Skelmod capacitors were added as the extra storage potential was not warranted. Nevertheless, the new configuration has the ability to fit up to nine capacitors if a greater storage supply was needed for future applications.

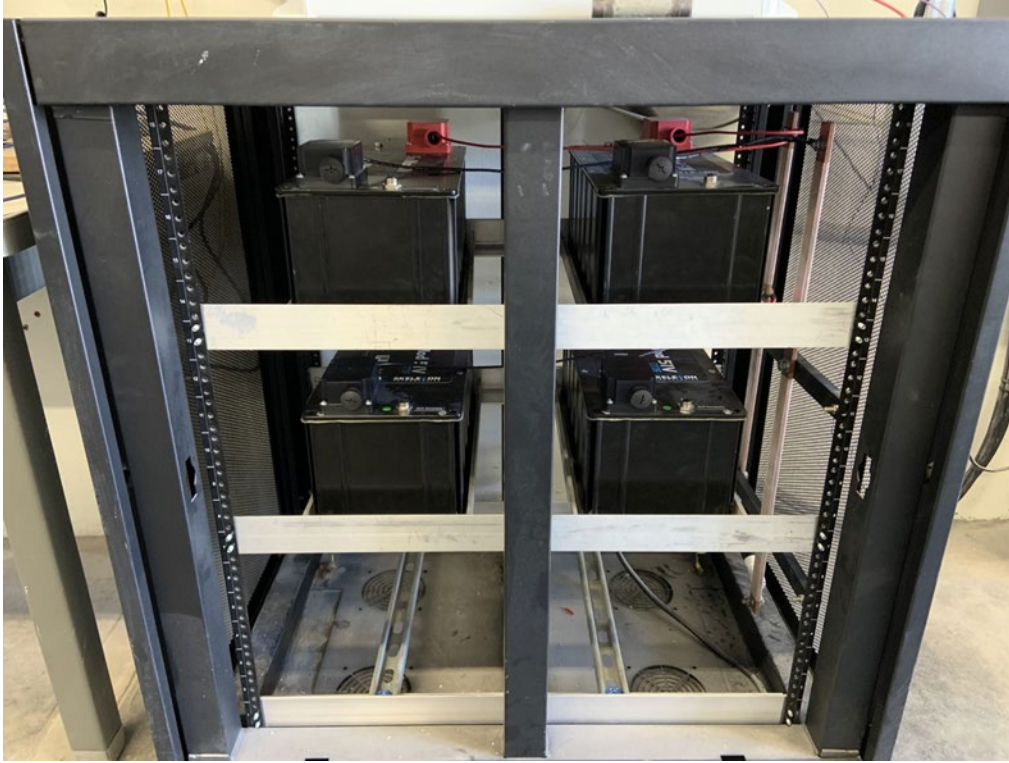


Figure 15. Updated Capacitor Configuration (side view).

The placement of the capacitors in this manner also aligned the positive and negative terminals on two distinct sides, simplifying the wiring and bus bar configuration needed. However, the top oriented ring terminals on the new capacitors were not conducive to supporting the copper bus bars. Plastic structural supports were cut and bolted into the side mounts in order to hold the modified bus bars while insulating the metal housing structure from the capacitors. Each terminal was wired with crimp connectors and attached to various points on the bus bars. The microgrid connections were attached at the base of each bar. The final configuration is picture in Figure 16.



Figure 16. Updated Capacitor Configuration (front view).

III. AIR MOTOR CONFIGURATION

A. MOTOR GENERATION MODULE

The motor used to power the electrical generator is an AirPro UTAM4-030S Radial Air Motor developed by AirOil Systems. The motor features a five-piston cylinder configuration as the primary driving mechanism for the shaft and electric generator.

A schematic of the motor and its operating curves from the manufacturer are included in Figure 17 and Figure 18, respectively. The motor itself and its electrical components are representative of what could soon be an off the shelf product for simple and effective electric generation.

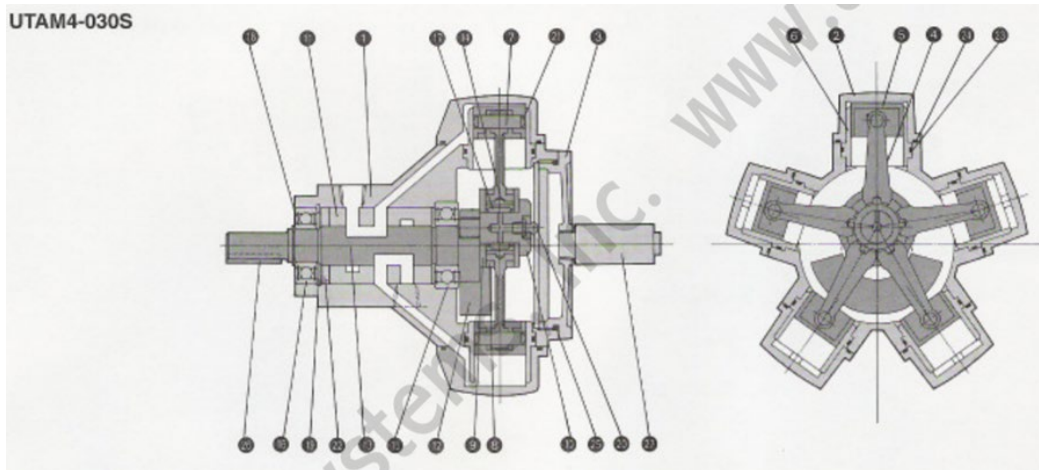


Figure 17. UTAM4-030S Cutaway Schematic. Adapted from [13].

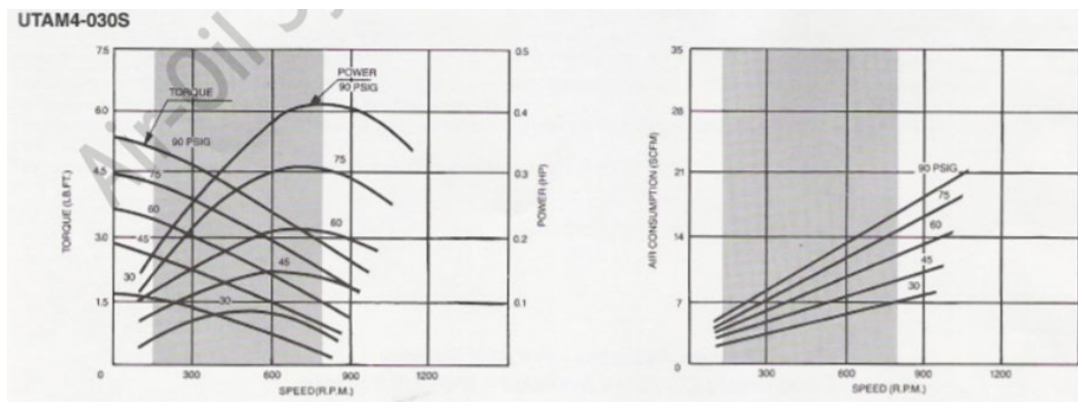


Figure 18. UTAM4-030S Operating Curves. Adapted from [13].

An 80 kV XOAR electric motor, used as a generator, three separate single-phase Emerson E200EWA transformers, and a MSD100-12 three phase rectifier complete the generator system as shown in Figure 19. This final configuration is the result of significant testing by Johnson and is similar to past iterations [9].

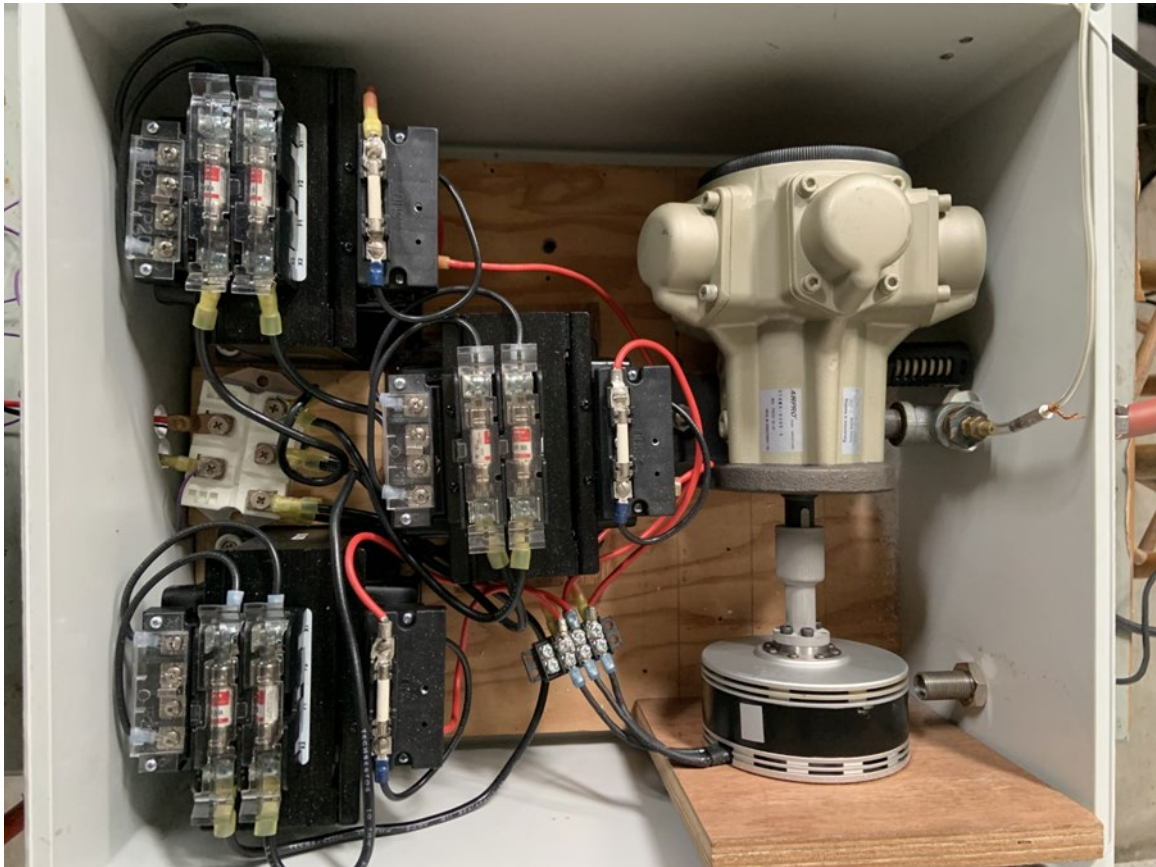


Figure 19. Air Motor Assembly.

B. CONTROL MANIFOLD

The expansion system could produce electricity from compressed air but had no means of regulating its output. Thus, a control manifold originally developed by Vranas was adopted as the plumbing structure for the motor.

The air coming from the supply line would diverge in the split structure shown in Figure 20 and then proceed through one of the two channels to the motor. This design

featured two Parker B6 Series solenoid valves, one manual Apollo 71–502 Series valve, and two Crydom D2450 solid-state relays for solenoid activation [10].

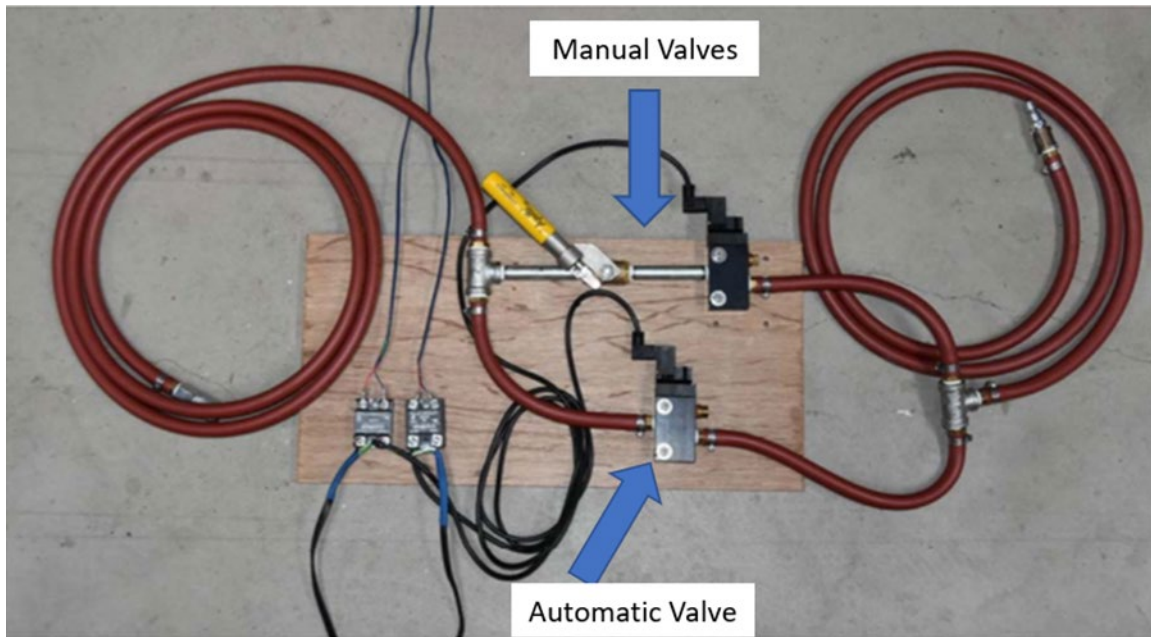


Figure 20. Expansion Control Manifold. Adapted from [10].

THIS PAGE INTENTIONALLY LEFT BLANK

IV. MOTOR CHARGE CHARACTERISTICS AND CONTROL

A. MOTOR INSTRUMENTATION

With the addition of new capacitors and a change in the air supply line being used, the motor's charge characteristics were re-explored. Johnson's original tests evaluated an 80 kV and 150 kV electric motor's ability to bring a single drained capacitor up to its full charge. The results indicated that the 80 kV generator provided the best efficiency and charge time, resulting in the final motor configuration discussed previously [9].

A CR5311-75 voltage transducer, pressure line, and Monarch optical sensor were attached to the motor system to collect voltage, pressure, and motor speed data over the course of the test run. The instrumentation setup in Figure 21 resulted in no interference to normal motor operation.

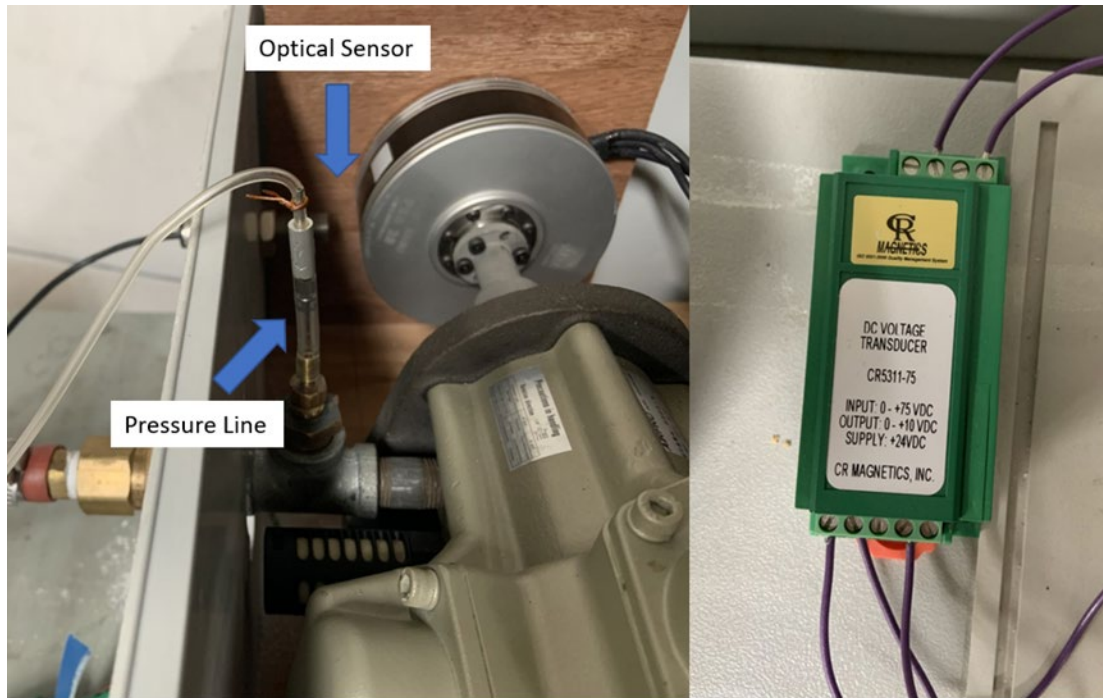


Figure 21. Motor Side Data Acquisition.

A NI Multifunction I/O DAQ and DSA 3217 pressure brick were used to collect the incoming data and transfer it to the computer. The connections for each piece of equipment are shown in Figure 22. The NI DAQ received the analog signals from both the optical sensor and transducer and transferred them through a USB connection. The pressure brick passed on its readings through an Ethernet connection.

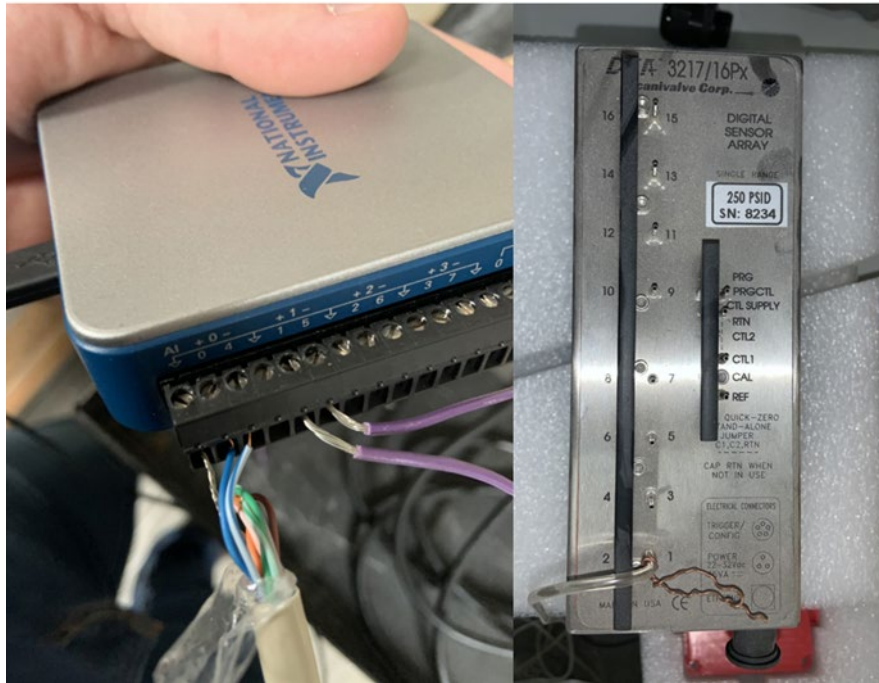


Figure 22. Computer Side Data Acquisition.

B. TESTING

Johnson's test was repeated by bringing a single Skelmod capacitor from a discharged state to 51 V. The new supply line regulated the compressed air pressure down within the motor's operating range before reaching the control manifold. Air was sent through the motor and powered the electric generator. A direct connection from the rectifier to the capacitor provided the charging path for the test as well as the connection for voltage readings. Two of Johnson's MATLAB scripts for recording and post-processing the data were adapted for the test run and are included in Appendix A [9]. The subsequent charge plots produced are discussed in the results section.

C. SYSTEM CONTROLLER

Successful charging of a single capacitor verified the motor's generation ability and charging characteristics. Before the physical integration of the air motor and generator into the microgrid, an initial control code was constructed to validate the control manifold's ability to regulate air flow. This allowed familiarity and practice with the Connected Components Workbench language used to program the Allen Bradley Micro 850 Programmable Logic Controller which is used as the PLC for the microgrid as well.

The Micro 850 in Figure 23 is shown in its base form. This specific model has a total number of twenty digital I/O voltage channels as well as an Ethernet port that supports TCP and Modbus communications.



Figure 23. Allen Bradley Micro 850 PLC.

An analog voltage/current plug-in module was added to the controller to read the incoming voltage signals from transducer previously attached. Figure 24 depicts the input voltage connections and the output channels used to control the solenoid valves.

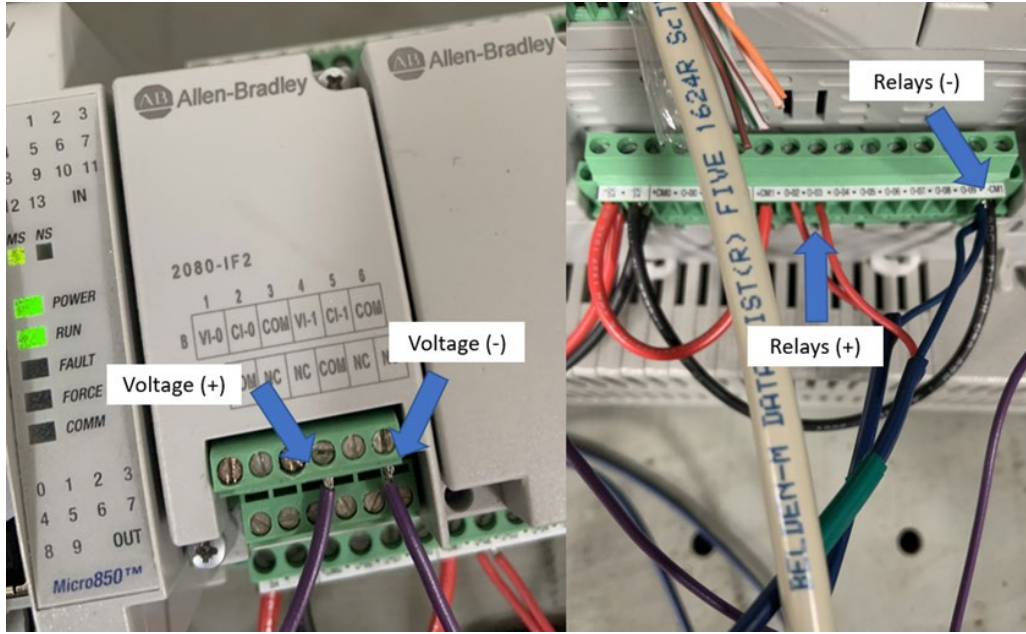


Figure 24. Micro 850 Wired Connections.

D. INITIAL EXPANSION CODE

The two separate pathways, with their corresponding valves and relays, allowed for the automated charging of the capacitor as well as provided the means of “Dark-starting” the system. This concept entails the system’s ability to be brought online without external power and is a critical factor that was applied in the final microgrid design. The control code used with this setup relied solely on the voltage input from the capacitor. The analog signal from the transducer was converted back into its real number form to be used in the main control program.

Vranas’ solution used the SCALER function to achieve this, and the resulting block form sub-program is pictured in Figure 25 [10].

The same conversion approach was used in the new control code; however, the SCALER function, along with the main control code, was written in text-structure for simplicity. While it may not be the apparent choice in this limited depiction, structured text provides a much more concise and coherent code as programs become more complex. The new SCALER function is included in Figure 26 with the main control code found in Appendix B. The SCALER function has five specific input variables, four of which

remained constant for this sub-program. The first set corresponded to the analog range potentially seen by the controller. Being a 12-bit system, this ranged from 0 to 4096 (2^{12}). The second set was the 0 to 75 input voltage range specified on the transducer. The final input was the actual analog signal seen by the _IO_P1_AI_01 channel on the controller. The resulting value was attached to the VolCap variable. It is important to note that although the controller is designated as a 12 bit system, its input data range is quoted to accept an input range of 0 to 65536. This corresponds to a 16 bit resolution which was utilized by Vranas in his control code [10].

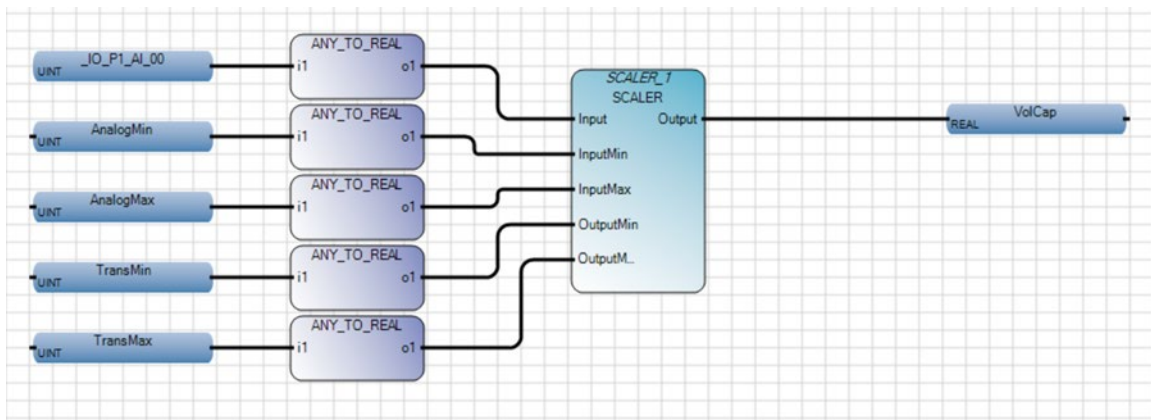


Figure 25. Block Form SCALER Function. Source: [10].

```

Micro850-VAR    Local Variables-VAR    V_Scale-POU  X V_Control-POU    Local Variables-VAR    Start Page    Micro850
1 SCALER_1(Any_To_Real(_IO_P1_AI_01),SCALER_1.InputMin,SCALER_1.InputMax,SCALER_1.OutputMin,SCALER_1.OutputMax);
2 VolCap := SCALER_1.Output;
3

```

Figure 26. Structured Test SCALER Function.

The same conversion approach was used in the new control code; however, the SCALER function, along with the main control code, was written in text-structure for simplicity. While it may not be the apparent choice in this limited depiction, structured text provides a much more concise and coherent code as programs become more complex. The new SCALER function is included in Figure 26 with the main control code found in Appendix B. The SCALER function has five specific input variables, four of which remained constant for this sub-program. The first set corresponded to the analog range

potentially seen by the controller. Being a 12-bit system, this ranged from 0 to 4096 (2^{12}). The second set was the 0 to 75 input voltage range specified on the transducer. The final input was the actual analog signal seen by the `_IO_P1_AI_01` channel on the controller. The resulting value was attached to the `VolCap` variable. It is important to note that although the controller is designated as a 12 bit system, its input data range is quoted to accept an input range of 0 to 65536. This corresponds to a 16 bit resolution which was utilized by Vranas in his control code [10].

The main control program was made up of five separate if else statements used to actuate the necessary relays and solenoid valves. When the controller is online and the measured voltage level is below the maximum, the `_IO_EM_DO_02` channel connected to the automatic solenoid valve will activate. This will allow air from the supply line to flow into the motor and begin charging the capacitor. Once it reaches full charge, the automatic valve will close and the initially true Boolean variable `MotorFlipFlop` will shift to false. This variable prevents the motor from continuously cycling on and off every time the voltage level drops slightly from its maximum value. Instead, a minimum voltage of 40 VDC was arbitrarily chosen as the value to begin charging the capacitor again. If `MotorFlipFlop` is false and the voltage drops below the assigned 40 VDC, the automatic solenoid valve will be activated again until the capacitor is fully charged.

The manual and automatic side of the control manifold is made possible by the initial states of the solenoid valves. The automatic side features a solenoid valve that will remain closed until it receives power. The manual side features the opposite with the valve closing upon its activation. These qualities allow for the previously mentioned “dark-start” of the system and was coded for such application in the control program. If the controller is offline and no source of power is readily available, the manual lever valve could be utilized to let air flow into the motor. Once the capacitor gains sufficient charge and the controller comes online, the `_IO_EM_DO_03` channel of the manual side solenoid valve will be activated. The program controlling the automatic solenoid valve will take over, and the system will self-regulate. The closing of the manual side solenoid valve is a safety mechanism put in place to prevent the overcharging of the capacitors by an operator keeping the inlet valve open.

V. MOTOR INTEGRATION AND MICROGRID CONTROL

A. AIR MOTOR CONNECTION

After initial automation and testing, the expansion module and control manifold were wired into the microgrid. The air motor connection made use of the previous power supply setup implemented by Tan [8].

The power supply's positive terminal was originally connected to a diode to prevent electrical backflow. This diode then fed into a solid state relay that would control the connection to the capacitor bank and microgrid as a whole. Figure 27 shows the previous connections in detail.

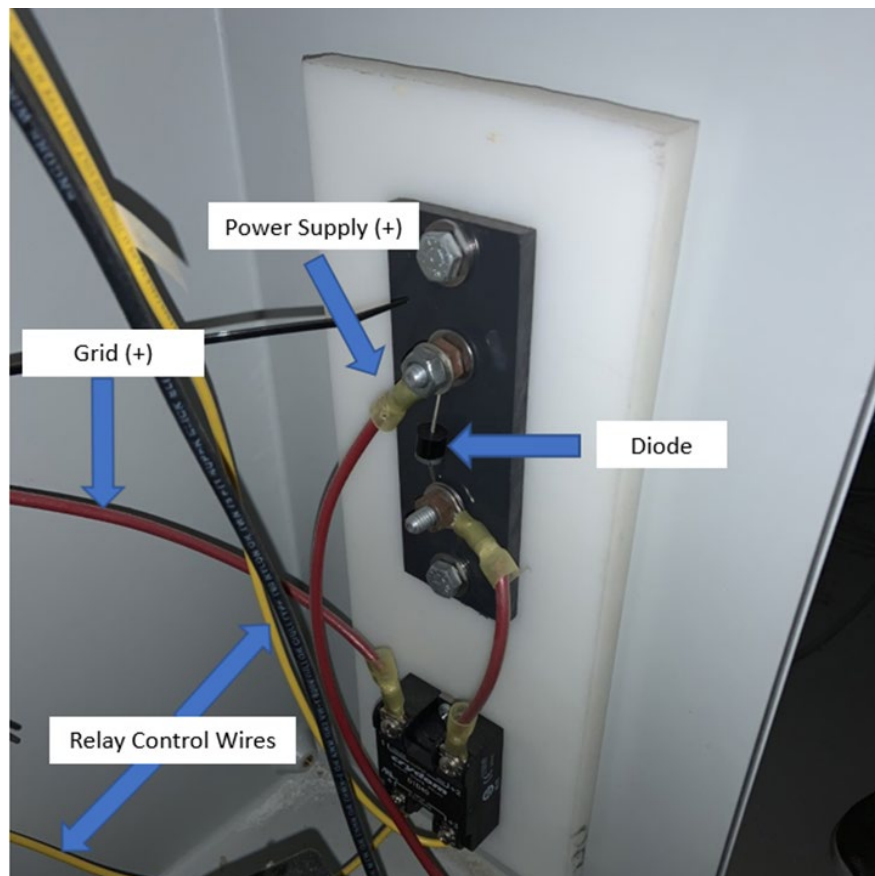


Figure 27. Previous Power Supply Connection.

The diode was kept for the aforementioned purpose when setting up the motor connection. The positive terminal on the motor rectifier was wired to the top of the diode, and the microgrid's negative connection was wired to the rectifier's negative terminal. The previously used solid state relay was bypassed, with the microgrid's positive connection wired directly to the bottom of the diode. The simplified setup is pictured in Figure 28.



Figure 28. Motor-Grid Connection.

The solid state relay was made obsolete by the two relays already attached to the control manifold that powered the solenoid valves. The manifold's automatic valve relay connection utilized the same `_IO_EM_DO_09` channel as power supply relay. The manual valve connection was wired to the adjacent `_IO_EM_DO_08` channel. Thus, the means of controlling capacitor voltage levels changed from regulating the electrical connection to regulating the compressed air flow. The overall expansions setup, to include wiring and tubing, is included in Figure 29.

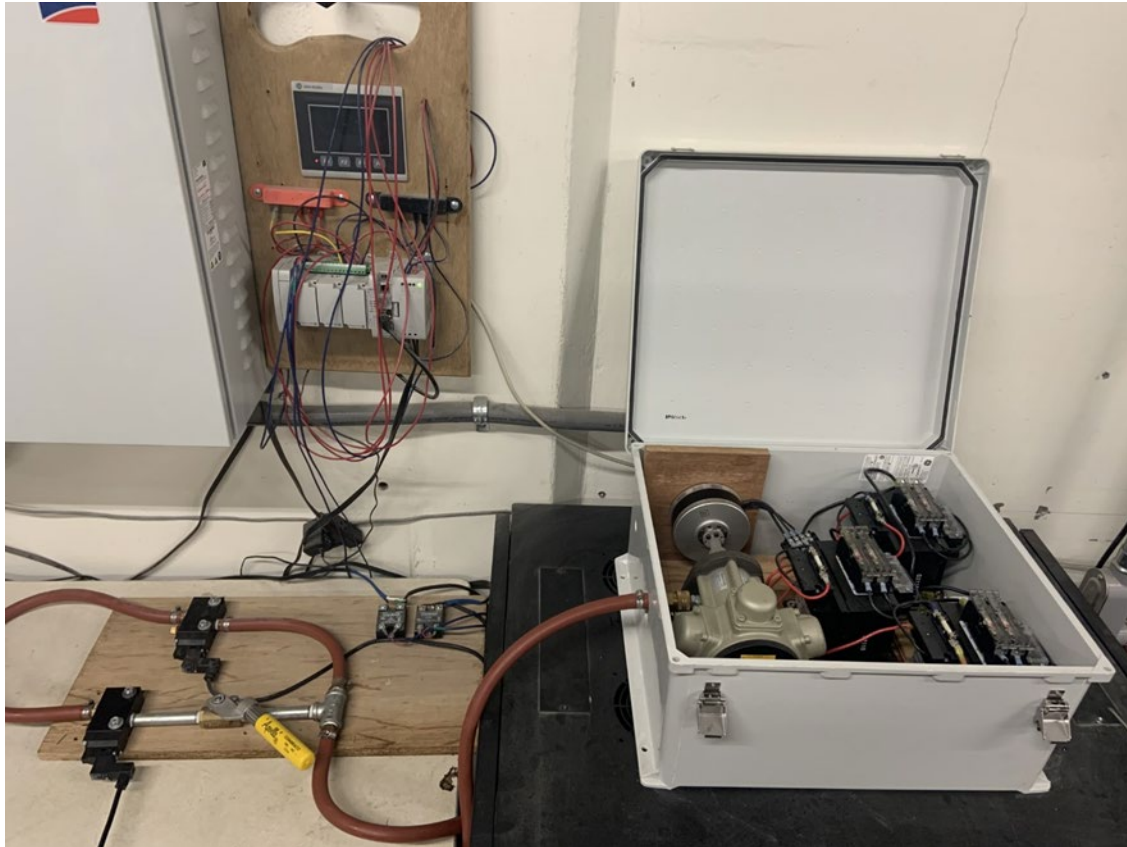


Figure 29. Controller, Manifold, and Motor Setup.

B. CONTROL MODIFICATIONS

The bulk of the microgrid's control code was left untouched as it had no effect on the expansion system. The `Activate_PowerSupply` subprogram became the focus for motor control. Since Tan utilized his SSR in a similar manner to the relays on the control manifold, the code could be modified and reused.

The subprogram in question is displayed in Figure 30. A major difference in the function of the microgrid control code and the single capacitor setup is the monitoring of the system's voltage. The initial expansion control utilized a transducer to directly read the capacitor voltage, while the microgrid controller received this parameter through the Midnite Classic 150 charge controller. The charge controller is able to communicate the capacitor and solar panel voltage levels through a Modbus protocol transferred through an Ethernet connection. This distinction is important as the Allen Bradley PLC receives no

voltage reading when the Midnite Classic goes offline. This occurs if the capacitors drop below 9–10 V.

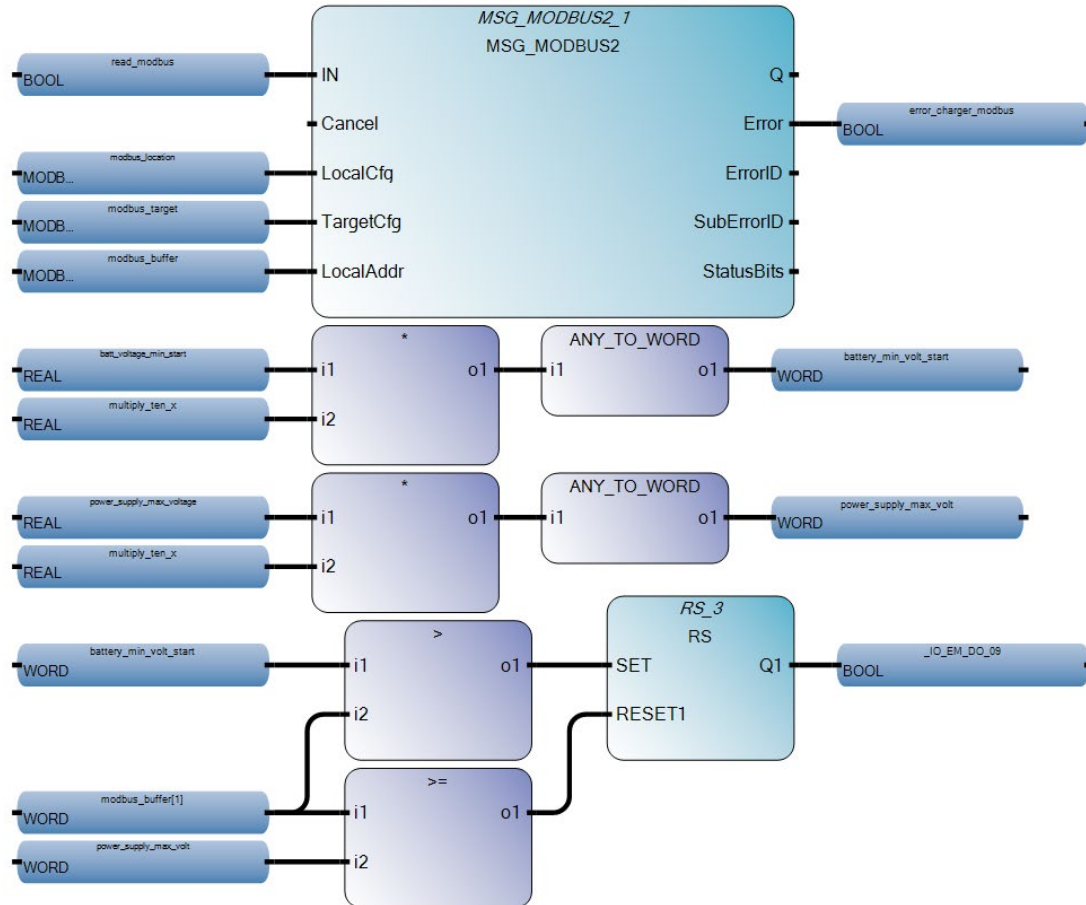


Figure 30. Activate_PowerSupply Sub-Program. Source: [8].

This primarily affects the manual valve operation when attempting to “dark-start” the system after a complete shutdown. The initial expansion code closed the manual side solenoid valve once the PLC gained power and began regulating the automatic valve. If this approach was used, the manual valve would shut before the Midnite Classic could come online and provide the voltage readings to the PLC for automation. A simple fix involved waiting to actuate the manual valve until the PLC read a voltage level of 10 V or greater. This would allow the initial “dark-start” charging and prevent any overcharging once the capacitors reached their maximum voltage.

The automatic control comparative block from Figure 30 works in the same manner as the initial expansion code and can be used as is for the air motor. It receives its voltage reading from the Midnite Classic through the `modbus_buffer(1)` variable. If it falls below the `battery_min_volt_start` value, the `_IO_EM_DO_09` channel will activate allowing air to flow into the motor and charge the capacitors. Once the `power_supply_max_voltage` value is achieved, the channel is deactivated and will not turn on again until the voltage drops below the set range.

This range was originally set at 33–35.2 V. The lower end was based on the inverter shutdown voltage, and the upper end targeted the maximum voltage the power supply could provide. The air motor eliminated that restriction, and the value was changed to 50 V. The 1 V difference from the capacitors maximum value provided an additional buffer to prevent overcharging. The modified subprogram, now named, ‘Activate_AirMotor,’ is displayed in Figure 31 in block logic to conform with the overarching code structure. It includes the modification of the automatic side variables as well as the addition of the manual valve safety shut-off.

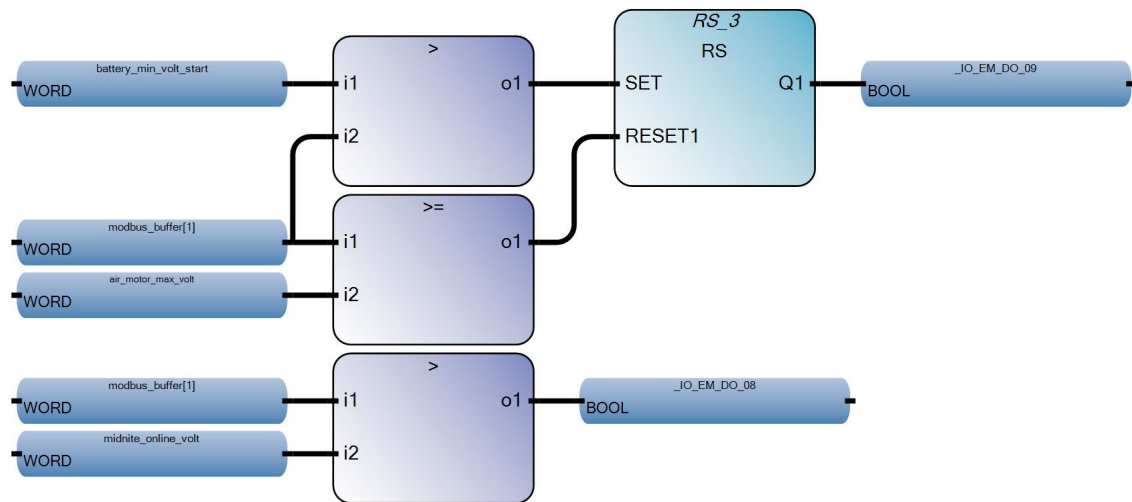


Figure 31. Activate_PowerSupply Sub-Program Modifications.

C. EXPERIMENTAL TESTING

Two experiments were performed to evaluate the performance of the air motor and then its integration into the microgrid with results presented later. The first experiment used the air motor to charge a single supercapacitor from zero to its rated voltage while monitoring its performance to calculate the combined efficiency of the air motor and generator.

The final verification for the newly integrated SS-CAES microgrid was to track the capacitor voltage over night as it discharges to see if the motor would function properly and maintain the specified voltage range. Midnite Solar's Local Status Panel app allowed for an additional Ethernet connection to the charge controller during operation. Once data acquisition was authorized in the app, the program tracked numerous parameters related to the solar panels and storage medium. Individual parameters could be selected and plotted in the software or exported as an excel file. Acquisition and plotting steps are provided in detail in Appendix C.

VI. RESULTS AND DISCUSSION

A. MOTOR CHARGE RESULTS

Charging a single capacitor with the air motor system resulted in charge characteristic plots similar to Johnson's original tests. The same efficiency calculations were conducted for the new setup for comparison.

The voltage plot in Figure 32 shows that it took the air motor 25 minutes to raise a completely discharged capacitor to 51 V. This maximum voltage was used in Equation 1 to calculate the maximum stored energy of the capacitor in Joules.

The current and power curves depicted in Figure 33 and Figure 34, respectively, were derived from the voltage plot over the course of the run. The specific code that achieved this can be found in Appendix A. Figure 33 shows a relatively steady decrease in output current as the capacitor charged. The initial spike and oscillation are a result of the capacitor being completely discharged, leading to an inrush current once the connection was opened. Figure 34 shows that the motor's output power levels of around 190 watts near full charge.

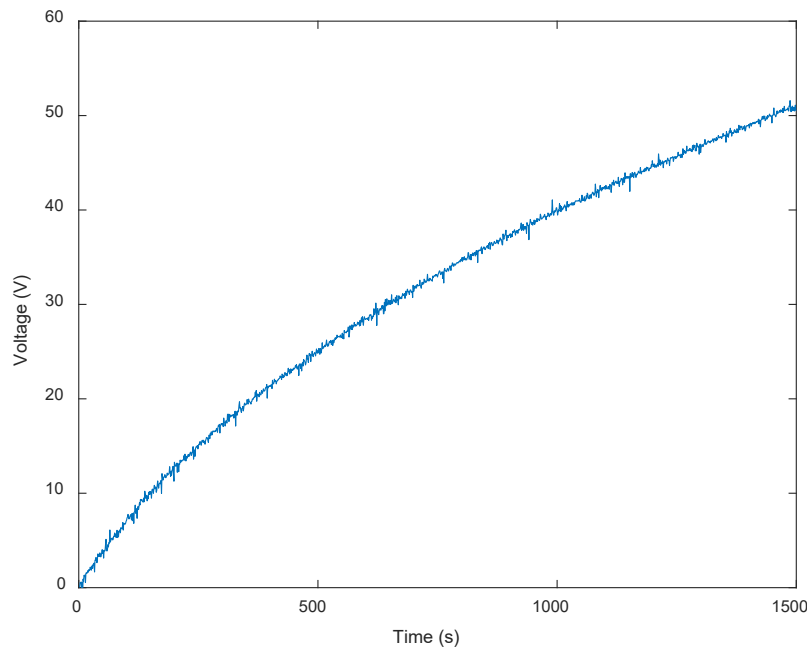


Figure 32. Plot of Voltage vs. Time.

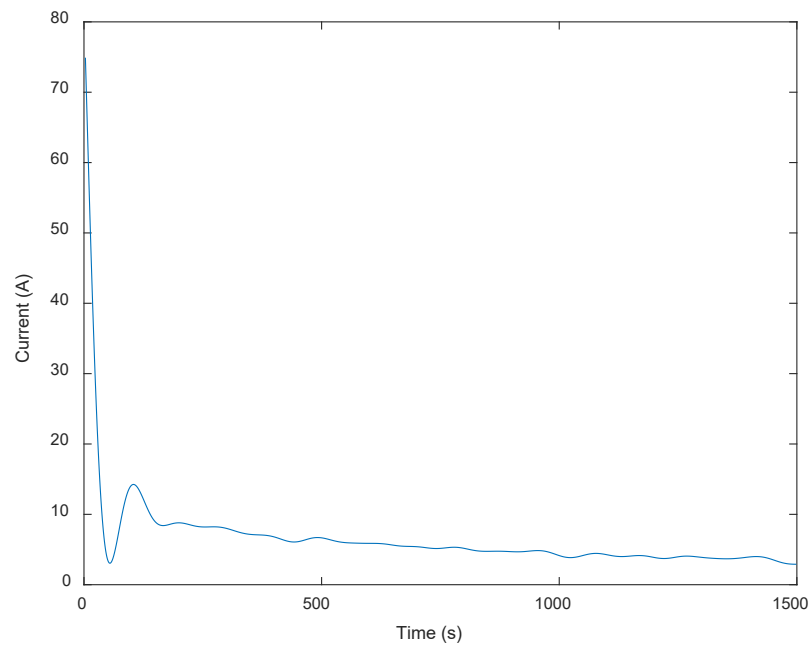


Figure 33. Plot of Current vs. Time.

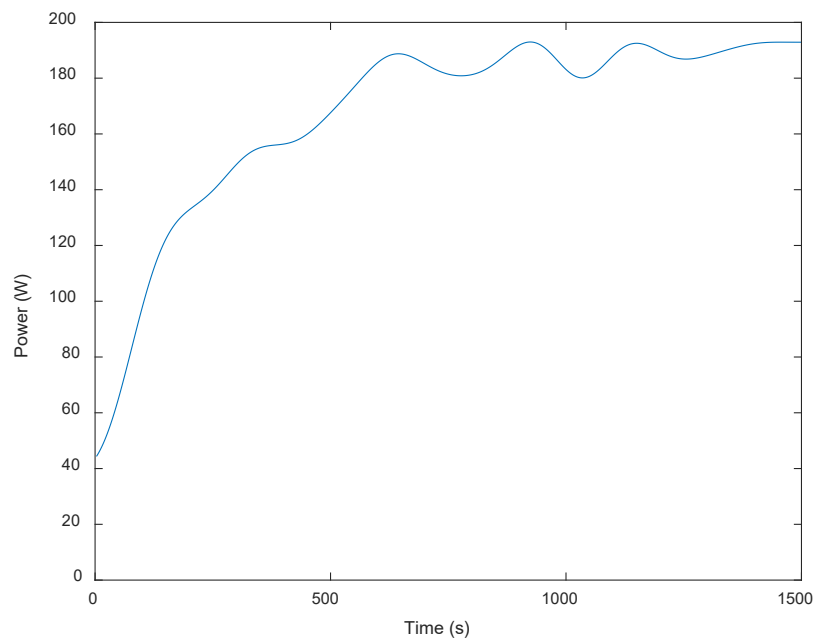


Figure 34. Plot of Power vs. Time.

One of the significant changes from Johnson's test was the supply air's inlet pressure into the air motor. The new supply line was regulated down to the pressures seen in Figure 35, while Johnson's pressures were kept at a value around 105 psig [9].

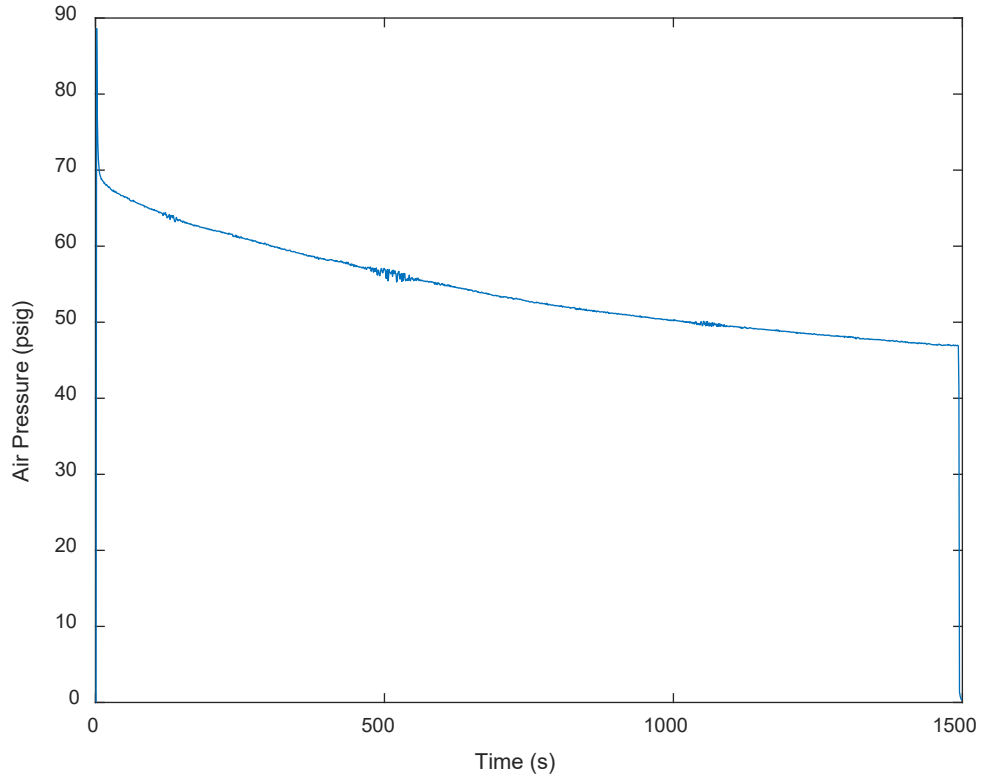


Figure 35. Plot of Air Pressure vs. Time.

This reduction of inlet pressure also reduced the overall motor speed during the test as shown in Figure 36. The combination of motor speed and inlet pressure were used to find the volumetric flow rate of air through the motor from the operating curves in Figure 18. This was then converted to volume by multiplying by the total test run time. Using this volume and the density of air at STP conditions in Equation 2 resulted in the total mass of air passed through the motor.

$$m = \rho V \quad (2)$$

Equation 3 allowed the calculation of the exit air temperature with three key assumptions. Namely, the expansion through the motor was isentropic, the exit pressure

was assumed to be atmospheric, and the inlet temperature of the supply line was taken at room temperature.

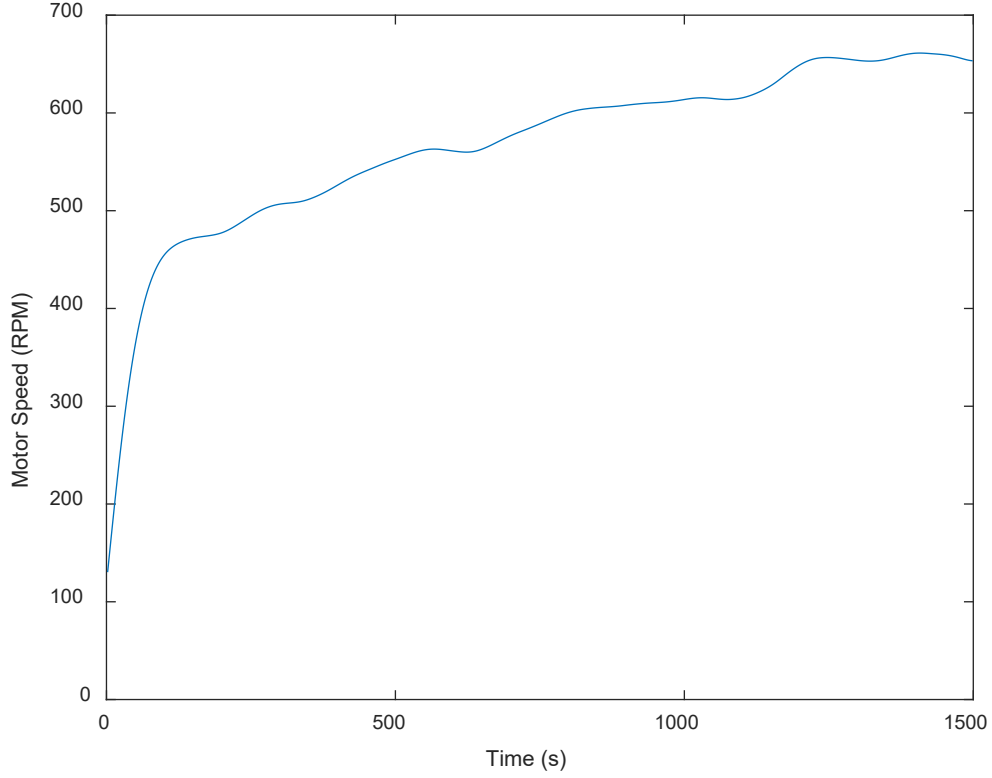


Figure 36. Plot of Motor Speed vs. Time.

$$T_2 = T_1 \left(\frac{p_2}{p_1} \right)^{\frac{\gamma-1}{\gamma}} \quad (3)$$

Equation 4 details the total energy that was used over the course of the test run to charge the capacitor. It involves multiplying the total fluid mass, the specific heat capacity of air, and the temperature differential from the inlet to the exit.

$$E_{in} = mc_p (T_1 - T_2) \quad (4)$$

Equation 5 shows the final step in calculating the efficiency of the system by taking the ratio of total capacitor energy over total energy used.

$$\eta = \frac{E_{stored}}{E_{in}} \quad (5)$$

B. DISCUSSION

The test run resulted in the use of 7.44 kg of air and an efficiency of 28.3%. The new setup was almost 13% more efficient than Johnson's original, but the increase was most likely due to the lower operating pressure seen during the test rather than the new capacitors. This is because the previous test was conducted at a pressure 15 psi over the maximum operating pressure recommended by the manufacturer. While this setup was more efficient, it took almost double the time to fully charge the capacitor due to the lower motor speeds. Additionally, the high initial inrush current through the capacitors and torque on the motor could prove undesirable in a larger system but can easily be addressed by throttling the air supply on the manual side.

C. MICROGRID RESULTS AND DISCUSSION

The initial results from the Local Status Panel app showed that the voltage never dropped below the threshold set in the control code. The newer capacitors withstood the slow voltage drain from the microgrid components unlike the previous units. The control code and charge controller were then altered to show the initial purpose of the expansion module should a larger load be applied in the future. The charge controller was set to limit the capacitors to 40 V, and the motor's upper threshold limit was reduced from 50 V to 35 V. However, these changes only shed light on a different issue. While the Local Status Panel app was data logging, it would continually hold open the connection to the charge controller. This produced an interference between the Midnite 150 and Micro 850, preventing the motor from being activated.

To circumvent the Ethernet interference, a direct voltage connection was made to the capacitor bank in the same manner as the motor charge test. The voltage levels through the course of the night were filtered and plotted in Figure 37.

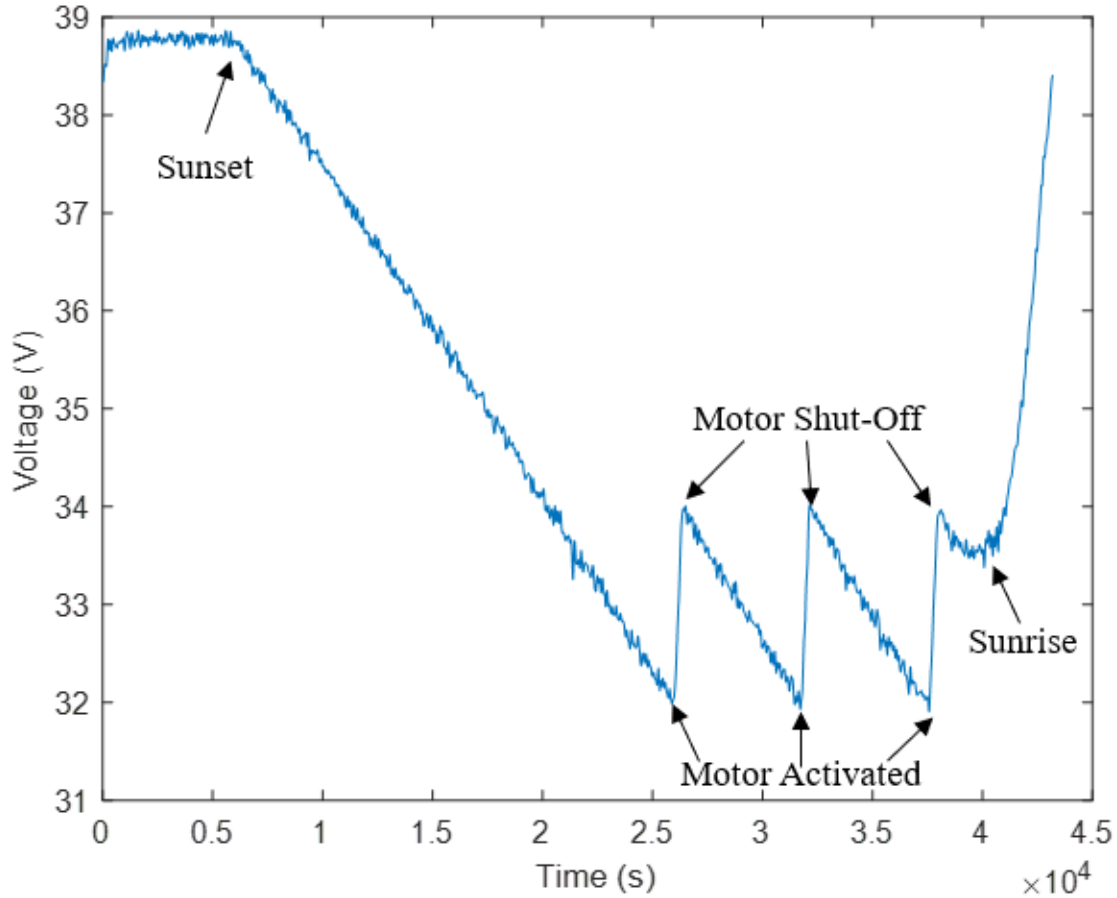


Figure 37. Microgrid Integration Verification.

D. DISCUSSION

The only issue found in the aforementioned method of recording was an approximately one volt difference between the transducer read voltages and the charge controller voltages. The disparity could potentially cause disruptions in the system operation near shut-down voltage levels for the various microgrid components or max voltage levels for the capacitors. Nevertheless, the curves indicate a successful control of the radial air motor throughout the night, and the inverter remained online. Specific voltage levels could be adjusted to remove any uncertainty in inverter shutdown or capacitor overcharge. The integration of the air motor into the microgrid for overnight charging has been demonstrated to be fairly straight forward using commercial off the shelf components. The one custom part required was the coupling between the air motor and generator.

VII. CONCLUSION

The successful integration of the expansion system with the SS-CAES microgrid brought together the work and design of numerous theses over the past few years. The expansion module features a robust and reliant method of electrical generation with an effective means of control through its plumbing manifold. Its addition to the microgrid allows for the overall system's continual use without fear of component shutdown. The upgrading of the capacitors adds to the durability of the microgrid and proves that newer capacitor technology is becoming a more viable candidate for energy storage. Most importantly, while the system remains operational at all times due to the addition of the new capacitors and expansion system, the ability to "Dark-start" the system should shutdown occur provides the greatest benefit to microgrid resilience.

THIS PAGE INTENTIONALLY LEFT BLANK

APPENDIX A. MATLAB CODES

A. DATA ACQUISITION

Main.m code in conjunction with JM_pbricksetup.m and JM_pbrickclose.m collect the voltage, pressure, and motor speed measurements and output voltage, current, power, pressure, and motor speed plots.

```
clear all
close all
clc

devices = daq.getDevices;
ni_set = daq.createSession('ni'); %creates connection with DAQ

ni_set.Rate = 4;

addAnalogInputChannel(ni_set,'Dev1',0:3,'Voltage');
for iii=1:numel(ni_set.Channels)
    ni_set.Channels(iii).TerminalConfig = 'Differential';
end

JM_pbricksetup; %connects with pressure brick code

vp = plot(NaN,NaN,'-');
pp = plot(NaN,NaN,'-');
rp = plot(NaN,NaN,'-');
ip = plot(NaN,NaN,'-');
pwrp = plot(NaN,NaN,'-');
Farad = 177; % Capacitor Farad Rating
```

Voltage Plot

```
subplot(5,1,1)
vp = plot(NaN,NaN,'-');
title('Capacitor Voltage')
xlabel('Time (s)')
ylabel('Voltage (DC)')
```

Current Plot

```
subplot(5,1,2)
ip = plot(NaN,NaN,'-');
title('Current')
xlabel('Time (s)')
ylabel('Current (Amps)')
```

Pressure Plot

```
subplot(5,1,3)
pp = plot(NaN,NaN,'-');
title('Air Pressure (PSI)')
xlabel('Time (s)')
ylabel('Pressure')
```

RPM Plot

```
subplot(5,1,4)
rp = plot(NaN,NaN,'-');
title('RPM')
xlabel('Time (s)')
ylabel('RPM')
```

Power Plot

```
subplot(5,1,5)
pwrp = plot(NaN,NaN,'-');
title('Power')
xlabel('Time (s)')
ylabel('Power (Watts)')
```

Data Collection

```
endtime = 1500;
hui= uicontrol('Style','edit','String',num2str(endtime));

iii=1;
while iii<endtime
    ni_set.DurationInSeconds = 1;
    event.data = startForeground(ni_set);
    fprintf(pbrick1, 'SCAN'); % this is just a reading function
    output = ws_readPressureBrickData(pbrick1,pbrickvars);
    Capvolts=(mean(event.data(:,1))*7.5)-.37;
    rpm = (max((event.data(:,2))*1000));
    rpm = filter(b,a,rpmx);
    Charge(iii) = Farad*Capvolts;
    if iii>1
        I = (Charge(iii)-Charge(iii-1))/1;
        set(ip,'xdata',[get(ip,'xdata') iii],'ydata',[get(ip,'ydata') I]);
        Power=((Capvolts*I));
        set(pwrp,'xdata',[get(pwrp,'xdata') iii],'ydata',[get(pwrp,'ydata') Power]);
    end

    set(vp,'xdata',[get(vp,'xdata') iii],'ydata',[get(vp,'ydata') Capvolts]);
    set(pp,'xdata',[get(pp,'xdata') iii],'ydata',[get(pp,'ydata') output.Pressures(1)/6890]);
    set(rp,'xdata',[get(rp,'xdata') iii],'ydata',[get(rp,'ydata') rpm]);
```



```

iii=iii+1;
endtime = str2double(get(hui,'String'));
end

ni_set.stop
JM_pbrickclose
%disband read connections

fname = 'TestRun';
csvwrite(fname,[get(vp,'xdata')' get(vp,'ydata')' get(pp,'ydata')' get(rp,'ydata')'
[0;get(ip,'ydata')]' [0;get(pwrp,'ydata')']])
%writes collected data to figure fname

```

Published with MATLAB® R2020b

B. DATA FILTER

DataFilter_Mod.m extracts that data from the 5 subplots produced from Main.m and filters out excess noise.

```

clear all
close all
clc

uiopen('C:\Users\jackm\Desktop\Thesis\Johnson\McMahan_test2.fig',1);
%Opens figure collected from Main.m

subplot(5,1,1) %references voltage subplot
kids = get(gca,'children');
x = get(kids,'xdata');
y = get(kids,'ydata'); %collects data from figure
figure(2)
plot(x,y) %plots voltage vs time
xlabel('Time (s)')
ylabel('voltage (V)')
ylim([0 60])

figure(1)
subplot(5,1,2)
kids = get(gca,'children');
x = get(kids,'xdata');
y = get(kids,'ydata');
figure(3)
x(1:2) = [];
y(1:2) = [];
[b,a] = butter(5,.02);
yyy = filtfilt(b,a,y); %filters noise out of plots
plot(x,yyy)

```

```

xlabel('Time (s)')
ylabel('Current (A)')
box on

figure(1)
subplot(5,1,3)
kids = get(gca,'children');
x = get(kids,'xdata');
y = get(kids,'ydata');
figure(4)
plot(x,y)
xlabel('Time (s)')
ylabel('Air Pressure (psig)')
box on

figure(1)
subplot(5,1,4)
kids = get(gca,'children');
x = get(kids,'xdata');
y = get(kids,'ydata');
figure(5)
x(1:2) = [];
y(1:2) = [];
[b,a] = butter(2,.009);
yyy = filtfilt(b,a,y);
plot(x,yyy)
xlabel('Time (s)')
ylabel('Motor Speed (RPM)')
ylim([0 700])
box on

figure(1)
subplot(5,1,5)
kids = get(gca,'children');
x = get(kids,'xdata');
y = get(kids,'ydata');
figure(6)
x(1:2) = [];
y(1:2) = [];
[b,a] = butter(5,.01);
yyy = filtfilt(b,a,y);
plot(x,yyy)
xlabel('Time (s)')
ylabel('Power (W)')
ylim([0 200])
box on

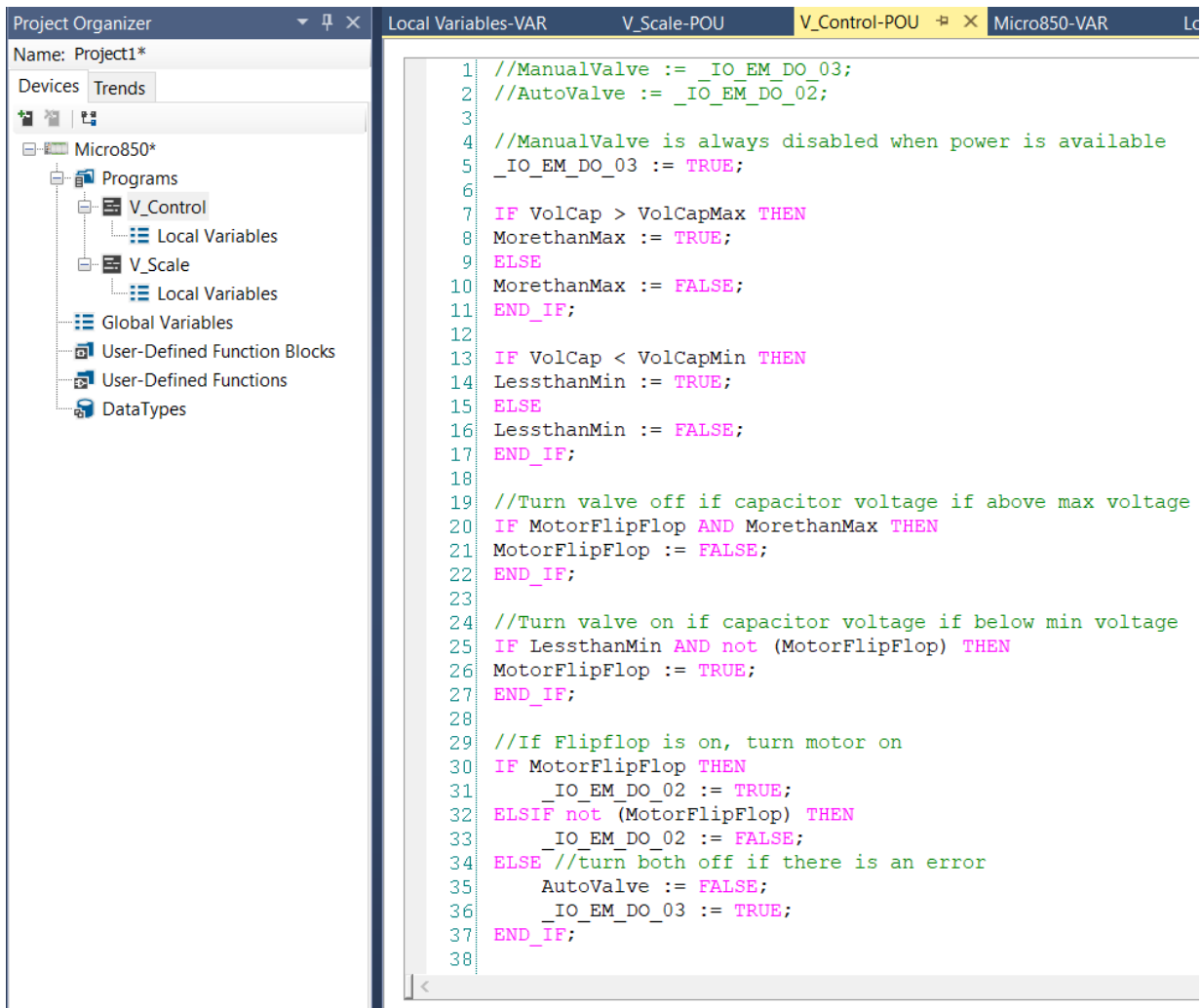
```

Published with MATLAB® R2020b

APPENDIX B. CCW CONTROL CODE

A. VOLTAGE CONTROL

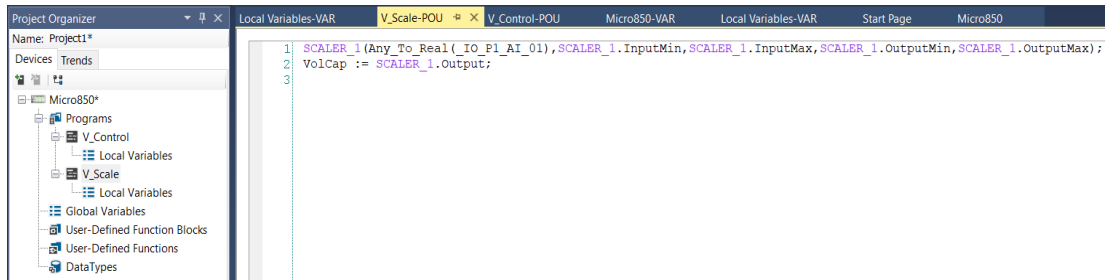
Project 1 is the initial expansion control of the air motor with a single capacitor. It uses an upper and lower voltage threshold to activate the automatic side solenoid valve.



The screenshot displays a PLC programming environment. On the left, the 'Project Organizer' shows a tree structure for 'Project1*'. Under 'Micro850*', there are 'Programs' and 'Trends'. The 'Programs' folder contains 'V_Control', 'V_Scale', and 'Local Variables'. The 'V_Control' program is selected. The main window shows the 'V_Control-POU' code editor. The code is written in a ladder logic style with comments and logical statements. The code is as follows:

```
1 //ManualValve := _IO_EM_DO_03;
2 //AutoValve := _IO_EM_DO_02;
3
4 //ManualValve is always disabled when power is available
5 _IO_EM_DO_03 := TRUE;
6
7 IF VolCap > VolCapMax THEN
8   MorethanMax := TRUE;
9 ELSE
10  MorethanMax := FALSE;
11 END_IF;
12
13 IF VolCap < VolCapMin THEN
14   LessthanMin := TRUE;
15 ELSE
16   LessthanMin := FALSE;
17 END_IF;
18
19 //Turn valve off if capacitor voltage if above max voltage
20 IF MotorFlipFlop AND MorethanMax THEN
21   MotorFlipFlop := FALSE;
22 END_IF;
23
24 //Turn valve on if capacitor voltage if below min voltage
25 IF LessthanMin AND not (MotorFlipFlop) THEN
26   MotorFlipFlop := TRUE;
27 END_IF;
28
29 //If Flipflop is on, turn motor on
30 IF MotorFlipFlop THEN
31   _IO_EM_DO_02 := TRUE;
32 ELSIF not (MotorFlipFlop) THEN
33   _IO_EM_DO_02 := FALSE;
34 ELSE //turn both off if there is an error
35   AutoValve := FALSE;
36   _IO_EM_DO_03 := TRUE;
37 END_IF;
38
```

B. VOLTAGE SCALE



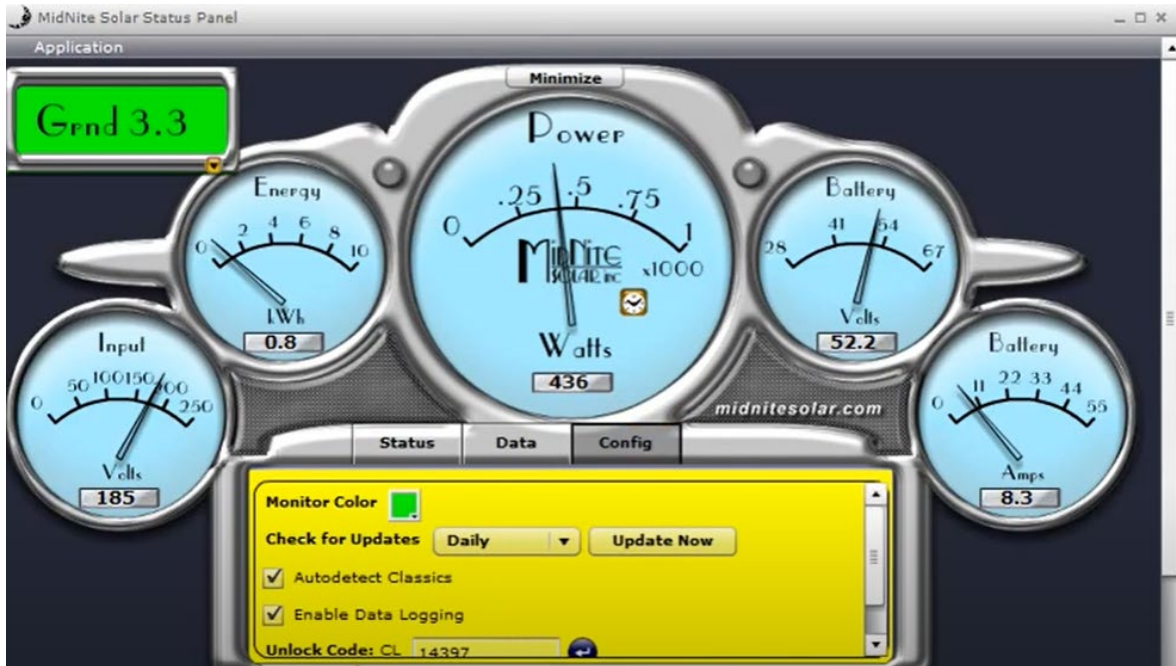
C. GLOBAL VARIABLES

Name	Alias	Data Type	Dimension	Project Val	Initial Value	Comment	String Size
_IO_EM_DO_00		BOOL	-	FALSE			
_IO_EM_DO_01		BOOL	-	FALSE			
_IO_EM_DO_02		BOOL	-	TRUE			
_IO_EM_DO_03		BOOL	-	TRUE			
_IO_EM_DO_04		BOOL	-	FALSE			
_IO_EM_DO_05		BOOL	-	FALSE			
_IO_EM_DO_06		BOOL	-	FALSE			
_IO_EM_DO_07		BOOL	-	FALSE			
_IO_EM_DO_08		BOOL	-	FALSE			
_IO_EM_DO_09		BOOL	-	FALSE			
_IO_EM_DI_00		BOOL	-	FALSE			
_IO_EM_DI_01		BOOL	-	FALSE			
_IO_EM_DI_02		BOOL	-	FALSE			
_IO_EM_DI_03		BOOL	-	FALSE			
_IO_EM_DI_04		BOOL	-	FALSE			
_IO_EM_DI_05		BOOL	-	FALSE			
_IO_EM_DI_06		BOOL	-	FALSE			
_IO_EM_DI_07		BOOL	-	FALSE			
_IO_EM_DI_08		BOOL	-	FALSE			
_IO_EM_DI_09		BOOL	-	FALSE			
_IO_EM_DI_10		BOOL	-	FALSE			
_IO_EM_DI_11		BOOL	-	FALSE			
_IO_EM_DI_12		BOOL	-	FALSE			
_IO_EM_DI_13		BOOL	-	FALSE			
VolCap		REAL	-	0.0			
ManualValve		BOOL	-	FALSE			
AutoValve		BOOL	-	FALSE			
MorethanMax		BOOL	-	FALSE			
LessthanMin		BOOL	-	TRUE			
VolCapMax		REAL	-	14.5	50.0		
VolCapMin		REAL	-	13.0	40.0		
MotorFlipFlop		BOOL	-	TRUE			
_IO_P1_AI_00		UINT	-	0			
_IO_P1_AI_01	0	UINT	-	15			
_SYSVA_CYCLECNT		DINT	-	4025912		Cycle counter	
_SYSVA_CYCLEDAT		TIME	-	T#28m36s42		Timestamp of the beginnin	
_SYSVA_KVBPERR		BOOL	-	FALSE		Kernel variable binding pro	
_SYSVA_KVBCERR		BOOL	-	FALSE		Kernel variable binding con	
_SYSVA_RESNAME		STRING	-	'CONTROLLE		Resource name (max length	
_SYSVA_SCANCNT		DINT	-	4025922		Input scan counter	
_SYSVA_TCYCYTIM		TIME	-	T#0s		Programmed cycle time	
_SYSVA_TCYCURRE		TIME	-	T#0s		Current cycle time	
_SYSVA_TCYMAXIM		TIME	-	T#3ms		Maximum cycle time since l	
_SYSVA_TCYOVERFI		DINT	-	0		Number of cycle overflows	
_SYSVA_RESMODE		SINT	-	3		Resource execution mode	
_SYSVA_CCEXEC		BOOL	-	FALSE		Execute one cycle when app	

APPENDIX C. LOCAL STATUS PANEL APP

A. ACQUISITION

Data logging under the configuration tab must be selected for continuous variable monitoring. The app must remain open for data to be acquired.



B. PLOTTING

Under the live tab, clicking values to chart allows the monitoring of several variables on the plot to include batter voltage (capacitor bank).



LIST OF REFERENCES

- [1] “Installation Energy Resilience Strategy,” Department of the Navy, last modified February 2020, <https://www.secnav.navy.mil/eie/Documents/DON-Installation-Energy-Resilience-Strategy.pdf>.
- [2] “Strategy for Renewable Energy,” Department of the Navy, last modified October 2012, <https://www.secnav.navy.mil/eie/documents/donstrategyforrenewable-energy.pdf>.
- [3] “Average U.S. construction costs for solar and wind generation continue to fall,” Energy Information Administration, last modified September 16, 2020, <https://www.eia.gov/todayinenergy/detail.php?id=45136>.
- [4] “Renewable account for most new U.S. electricity generating capacity in 2021,” Energy Information Administration, last modified January 11, 2021, <https://www.eia.gov/todayinenergy/detail.php?id=46416>.
- [5] “Compressed Air Energy Storage (CAES),” Climate Technology Centre & Network, accessed September 17, 2020, <https://www.ctcn.org/technologies/compressed-air-energy-storage-caes>.
- [6] He, W. and Wang, J., 2018, “Optimal selection of air expansion machine in Compressed Air Energy Storage: A review,” *Renewable and Sustainable Energy Reviews*, 87, pp. 77–95.
- [7] Williams, J., N., 2017, “Automated control of a solar microgrid-powered air compressor for use in a small-scale compressed air energy storage system,” M.S. thesis, Naval Postgraduate School, Monterey, CA.
- [8] Tan, H., 2019, “Industrial Control of a Supercapacitor and Compressed Air Storage System,” M.S. thesis, Naval Postgraduate School, Monterey, CA.
- [9] Johnson, M., S., 2020, “Small-Scale Energy Extraction for Compressed Air Energy Storage Using Positive Displacement Radial Air Motor,” M.S. thesis, Naval Postgraduate School, Monterey, CA.
- [10] Vranas, T., M., 2017, “Control system development for power generation from small-scale compressed air energy storage,” M.S. thesis, Naval Postgraduate School, Monterey, CA.
- [11] “Datasheet: SkelMod 51V,” Skeleton Technologies, accessed November 8, 2020, <https://www.skeletontech.com/skelmod-51v-ultracapacitor-module>.

- [12] “Datasheet: 56V Module,” Maxwell Technologies, accessed November 8, 2020 https://www.maxwell.com/images/documents/56vmodule_ds_1017119-3.pdf.
- [13] “UTAM4 Series Radial Piston Air Motor,” Air-Oil Systems, accessed November 5, 2020, <https://www.airoil.com/uploads/assets/downloads/airpromotor.pdf>.

INITIAL DISTRIBUTION LIST

1. Defense Technical Information Center
Ft. Belvoir, Virginia
2. Dudley Knox Library
Naval Postgraduate School
Monterey, California